SELF-ORGANISED CRITICALITY AND SEISMICITY

By

Leandro Boonzaaier

Thesis presented in partial fulfilment of the requirements for the degree of
MASTER OF SCIENCE at the University of Stellenbosch.

Supervisor : Professor H. B. Geyer

Co-supervisor : Dr. W. de Beer

December 2002

DECLARATION

I, the undersigned, hereby declare that the work contained in this thesis is my own original work and that I have not previously in its entirety or in part submitted it at any university for a degree.

ABSTRACT

In this thesis we give an overview of self-organised criticality and its application to studying seismicity. We recall some of the basic models and techniques for studying self-organised critical systems. We discuss one of these, the sandpile model, in detail and show how various properties of the model can be calculated using a matrix formulation thereof. A correspondence between self-organised critical systems and seismicity is then proposed. Finally, we consider the time-evolution of the sandpile model by using a time-to-failure analysis, originally developed in the study of seismicity and obtain results for the sandpile model that show similarities with that of the analyses of seismic data.

OPSOMMING

In hierdie tesis gee ons 'n oorsig van self-organiserende kritikaliteit en die toepassing daarvan in die studie van seismisiteit. Ons beskryf die basiese modelle en tegnieke vir die studie van self-organiserende kritiese sisteme. Ons bespreek een van hierdie, die sandhoopmodel, in besonderheid en wys hoe om verskeie eienskappe van die model te bereken deur gebruik te maak van 'n matriks-formulering daarvan. Ons stel dan 'n korrespondensie tussen self-organiserende kritiese sisteme en seismisiteit voor. Ter afsluiting ondersoek ons die tydontwikkeling van die sandhoopmodel deur gebruik te maak van 'n deurbreektyd analise wat oorspronklik in die bestudering seismiese data ontwikkel is. Die resultate vir die analise van die sandhoopmodel toon ooreenkomste met dit wat verkry word vir seismiese data.

CONTENTS

LIST OF TABLES

LIST OF FIGURES

ACKNOWLEDGEMENTS

I would like to acknowledge the contributions of the following people and institutions:

- My supervisor, Professor Hendrik Geyer, for his guidance and patience during this endeavour. Thank you for learning about SOC with me.
- My co-supervisor, Willem de Beer, for his input and insight into matters pertaining to seismicity and for his enthusiasm throughout this project.
- My family and friends for their support. Special thanks to Otini, Susan, Nicola, and Bryan for believing in me from the beginning and praying for me throughout. Tannie Rina and Allison for the encouragement during my time in the Free State and Carmen for believing in me these past few months.
- All the members of the ITF, both past and present, for creating an interesting working environment. It has been a pleasure working in and with the Theory Group at Stellenbosch. Special thanks to Andrew van Biljon and Lucian Anton for interesting discussions on life, the universe and physics in days gone by.
- The NRF, ISS International and the University of Stellenbosch for financial support.
- Most importantly, my Lord and Saviour, Jesus Christ, for life and the ability to understand.

Introduction

It has been known for some time that many natural phenomena occur via non-equilibrium processes. To date, however, there is not a single unified framework with which to study non-equilibrium systems. Self-Organised Criticality (SOC) represents one particular framework to study the behaviour of non-equilibrium systems [1]. It was introduced into statistical physics in 1987 by Bak, Tang and Wiesenfeld [5] in an attempt to explain the ubiquity of power-laws in nature. Many non-equilibrium natural phenomena are known to be characterised by probability distribution functions and correlation functions that have power-law behaviour. For example, earthquake sizes are distributed according to a power-law (the Gutenberg-Richter law) [2].

Bak, Tang and Wiesenfeld [5] introduced a simple cellular automaton (the so-called BTW sandpile model) in which power-law distribution functions of fluctuations emerge spontaneously without tuning any external parameters. From knowledge of equilibrium critical phenomena, we know that close to the critical point of continuous phase transitions, thermodynamical variables have power-law behaviour. Based on this, Bak et al. [5] suggested that power-law distribution functions in their model signalled that the system has reached a critical point. Hence the name self-organised criticality, because the criticality seemed to emerge spontaneously without explicit tuning of control parameters. The sandpile model represents a class of systems that are driven by some external source and respond to perturbations from it.

Soon after the proposal of SOC, many natural phenomena that were known to have power-law distributions, were analysed to see if they exhibited SOC behaviour. Amongst these, tectonic earthquakes have received much attention. It was soon suggested that tectonic earthquakes are indeed an example of systems displaying SOC behaviour since many of their observable features could be explained by using SOC [2]. Other systems, like real sand piles, were however found not to exhibit true SOC behaviour [9, 10, 11]. There was also a flurry of activity to establish what the essential features of SOC systems are and the conditions under which it is observed. This led to the introduction of many other models [6, 21, 22, 23] that were inspired by natural phenomena. Most of these models have been shown to exhibit SOC behaviour.

Although SOC has had some success in terms of giving a qualitative explanation for the behaviour of specific systems, there exists no general mathematical formalism that can account for the behaviour of such systems. This is unlike the situation in equilibrium critical phenomena where Renormalisation Group Theory has been very successful. Most of the attempts at constructing a mathematical theory of SOC have been somewhat ad-hoc and have only applied to

very specific model systems [7, 8, 20]. For the most part, SOC studies have been numerical.

The purpose of our study of SOC in this thesis is two-fold. Firstly, we attempt to extend the SOC-based analysis of earthquakes to those induced by human activity. While it is generally accepted that SOC provides a framework for earthquakes that occur naturally, it is not entirely obvious that it describes induced earthquakes. Secondly, we hope to gain some further understanding of the dynamics of SOC systems by explicitly considering the time-evolution of such systems. Power-law distribution functions seem to imply that the dynamical behaviour of a self-organised critical system is completely unpredictable since fluctuations on all scales are possible. We investigate whether there is some way in which one can extract information that will help with predicting the evolution on short time scales. Throughout the thesis we use the BTW model as our example of a SOC system.

The thesis is structured in the following way. In Chapter 1 we briefly recall the relevant ideas from equilibrium critical phenomena and then introduce Self-Organised Criticality. We also discuss the conditions under which SOC is observed by considering some examples. Chapter 2 gives an overview of the BTW sandpile model. We discuss the basic rules of the cellular automaton and the measurable properties of interest that quantify the system response to external perturbations. We then discuss some scaling relations between the exponents of the critical state and conclude the chapter with a brief description of variants of the BTW sandpile model.

In Chapter 3 we discuss an algebraic approach to the BTW model developed by Dhar [20]. This approach allows one to characterise the system in terms of the probabilities of configurations that the automaton can access in the critical state. This algebraic approach also provides a tool for calculating certain correlation functions in the critical state. We conclude Chapter 3 with a discussion on the connection between sandpile model configurations in the critical state and spanning trees on the square lattice.

Chapter 4 deals with the relation between SOC and induced seismic activity. The observable properties of induced seismicity are discussed and it is shown how one can explain it in terms of SOC. The results obtained by using the formalism presented in Chapter 3 form an integral part of this discussion.

In Chapter 5 we consider the dynamics of the sandpile model in detail. We give an overview of the time-to-failure analysis, which is a technique developed in the study of the large scale breakdown in disordered systems [37, 48]. This technique represents a framework with which to predict, on short time scales, when large breakdown events will occur in disordered systems. It is based on the hypothesis that large breakdown events are analogous to critical points of continuous phase transitions. We discuss its application to predicting large earthquakes in both

tectonic and mining-induced seismicity contexts. Based on the relation between seismicity and SOC systems, we apply the time-to-failure analysis to the BTW sandpile model and find that one can make qualitative statements concerning the time of occurrence of large events. We also discuss the conditions under which the time-to-failure analysis is valid. In Chapter 6 we conclude this work and discuss some remaining problems.

CHAPTER 1
Self-Organised Criticality

1.1 Introduction

In the introduction we said that the concept of self-organised criticality is defined analogously to that of equilibrium critical phenomena. We shall therefore start by first recalling some concepts from equilibrium critical phenomena and then define self-organised criticality, giving some examples.

1.2 Phase Transitions

We know from everyday experience that substances can exist in different phases under different conditions. For example, water can exist as a solid, liquid and a gas given the right conditions of temperature and pressure. In this section we give a brief description of how phase transitions between different phases of matter occur and the concepts used to describe these transitions [1].

Phase transitions occur when there is a singularity in some thermodynamic potential, such as the free energy. Consider the phase diagram of a typical liquid in Figure 1.1. We see that well-defined phase boundaries separate the different phases. Crossing the phase boundaries such as the liquid-gas in Figure 1.1, there is a jump in the densities (see Figure 1.2), which is a signature of a first-order transition. However, as the temperature is increased along the liquid-gas coexistence line, the difference in the liquid and gas densities decreases as we see from Figure 1.2. At the critical temperature, T_c, it becomes zero and beyond T_c it is possible to pass continuously from a liquid to a gas and vice versa.

Magnetic phase transitions show similar behaviour. Consider the phase diagram of a simple ferromagnet in Figure 1.3. Similar to liquid-gas transitions, there is a line of first-order transitions that ends in a critical point. Below T_c there is a jump in the magnetisation (Figure 1.5), but above T_c the transition from positive to negative magnetisation occurs continuously.

The density difference between the liquid and gas phases, $\rho_{liquid}(T) - \rho_{gas}(T)$, and the magnetisation, M, are examples of order parameters for the liquid and magnetic systems respectively. The order parameter is defined [3, 4] as a quantity that has the value of zero in the disordered phase and non-zero in the ordered phase. It gives a characterisation of the state of the system as it approaches the critical point. A specific order parameter for a given system is not uniquely defined. For the magnetic system we could have chosen M^3 for an order parameter as well. In

[1] See [3, 4] for excellent introductions to the theory of phase transitions

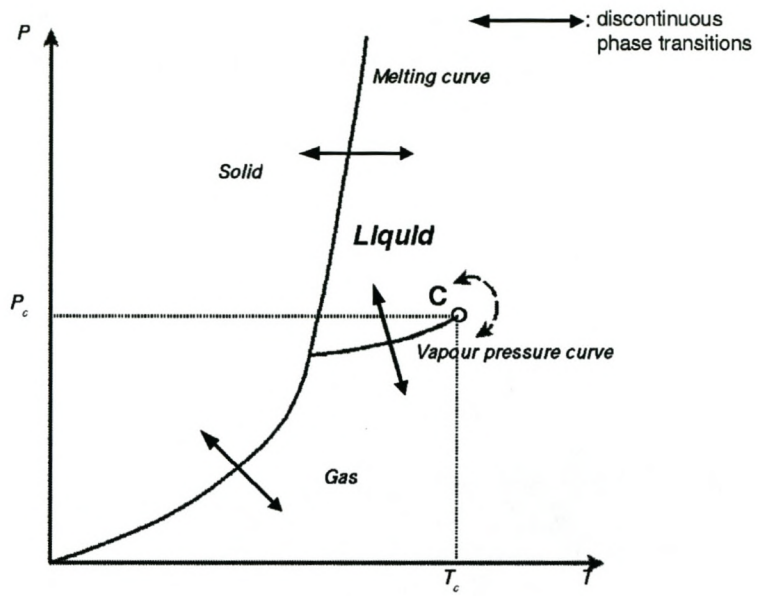

Figure 1.1: The pressure-temperature phase diagram of a typical fluid

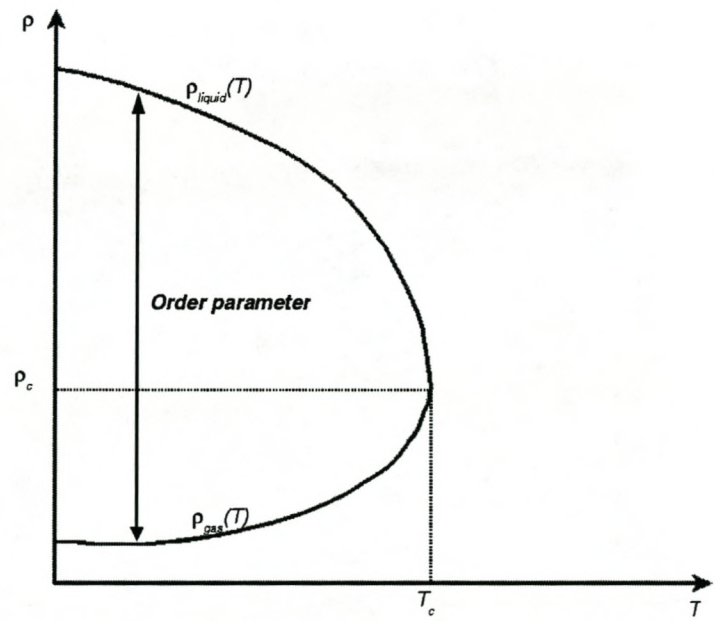

Figure 1.2: The values of the densities of liquid and gas on the coexistence curve

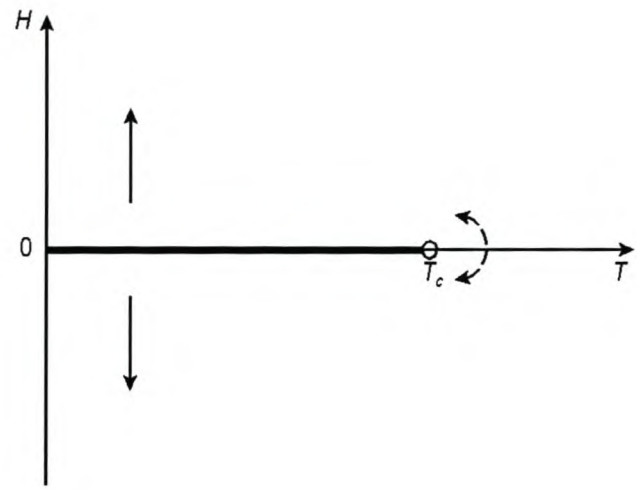

Figure 1.3: Phase diagram of a ferromagnet.

liquid and magnetic phase transitions the temperature is a control parameter that has to be tuned to observe these transitions.

We see that the line of first-order transitions ends in the critical point beyond which transitions become continuous. We mentioned above that phase transitions occur when there is a singularity in a thermodynamic potential. If there is a finite discontinuity in one or more of the first derivatives of the appropriate thermodynamic potential, the transition is said to be first-order. For a magnetic system the free energy, F, is the appropriate thermodynamic potential, with a discontinuity in the magnetisation ($M = -\left(\frac{\partial F}{\partial H}\right)_T$), below T_c, indicating that the transition is first-order (see Figure 1.5).

A transition is said to be continuous if the first order derivatives of the appropriate thermodynamic potential are continuous but second or higher order derivatives are discontinuous or infinite. Such transitions correspond to a divergent susceptibility, infinite correlation length and power-law correlations. The phase transition occurs as a result of the collective behaviour of the individual degrees of freedom. At the critical point the system as a whole has to be considered because of the diverging correlation length.

In the following section we describe some characteristics of continuous phase transitions by considering the example of the Ising model of ferromagnets.

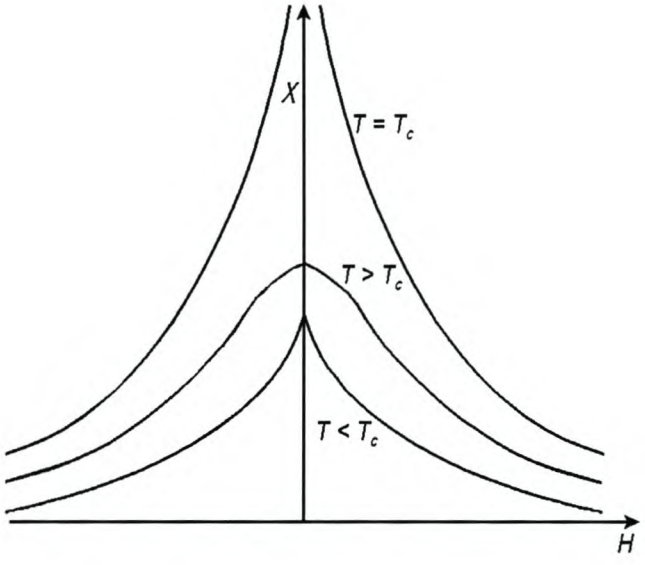

Figure 1.4: The magnetic susceptibility at different temperatures. Above and below T_c it is finite, but at T_c it diverges.

1.3 Ising model of ferromagnets

The Ising model is defined in terms of spins on the vertices of a lattice, labelled by indices $i = 1, 2, \ldots, N$. In this model the spins are restricted to point parallel or anti-parallel to one particular direction, say the z-axis. This is indicated by assigning the values $s_i = +1$ and $s_i = -1$ to spins that point parallel and anti-parallel to the z-axis, respectively.

Each spin is allowed to interact with its nearest neighbours with an interaction strength, J, which favours parallel alignment of spins. Each spin can also interact with other degrees of freedom such as external fields. The Hamiltonian of the model is given by

$$H = -h \sum_i s_i - J \sum_{<ij>} s_i s_j, \tag{1.1}$$

where $< ij >$ denotes a sum over nearest neighbours, h is the external magnetic field and J the interaction strength between nearest neighbour spins.

The two-dimensional model, at zero external field, was solved exactly by Onsager in 1944 and is furthermore known to have a phase diagram as shown in Figure 1.3 with a continuous transition at temperature T_c. The magnetisation becomes non-zero at T_c and increases continuously with decrease in T to its saturation value, which corresponds to all spins being aligned at $T = 0$ (see

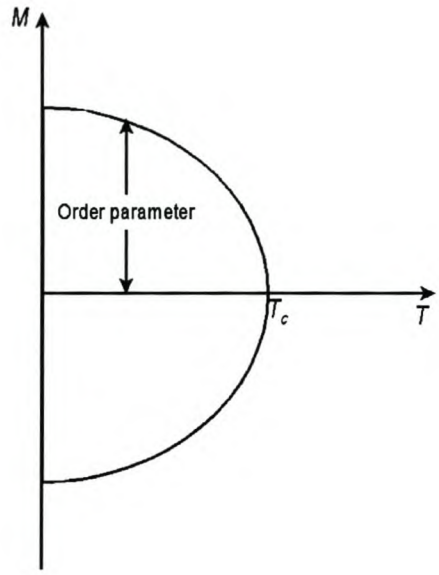

Figure 1.5: Magnetisation as a function of temperature.

Figure 1.5).

The behaviour of the individual spins is controlled by a competition between the contributions that the interaction, J, and entropy make to the interaction energy between the spins. At temperatures greater than T_c the entropy dominates and spin configurations are random. As the temperature is lowered the nearest neighbour interaction begins to dominate. Nearest neighbour spins start aligning and clusters of parallel spins start appearing.

The correlation length is a measure the size of the largest correlated clusters. Close to the critical temperature the correlation length is given by the expression

$$\xi \sim |T - T_c|^{-\nu}. \tag{1.2}$$

As the temperature is decreased the correlation length increases. The system shows interesting behaviour as the temperature is decreased. Not only does the correlation length increase, but small regions of clusters of correlated spins still appear. At the critical temperature itself, the regions of correlated spins range in size from a single spin to those of the size of the correlation length. We see from (1.2) that at T_c the correlation length becomes infinite.

The criticality of the system is embodied in the fact that even though the interactions are purely local, at T_c far-removed regions are correlated with each other. The critical point is thus

marked by two characteristics: an infinite correlation length and ordered structures on all length scales.

As a concluding remark we want to emphasize that the temperature has to be tuned explicitly to the special value of T_c to observe the interesting behaviour of a diverging correlation length and fluctuations on all length scales.

1.4 Self-Organised Criticality (SOC)

The study of out-of-equilibrium dynamics and heterogeneous systems has in recent years made the concept of complex systems popular. Systems with a large number of mutually interacting degrees of freedom that also exchange information or energy with their enviroment often have interesting macroscopic behaviour. Central to the study of complex systems is the potential for coherent large-scale collective behaviour which results from repeated non-linear interactions among the individual constituents.

Another aspect of complex systems that seems to be of central importance is that of punctuated dynamics. Punctuations correspond to rare and sudden bursts of activity that occur on time scales that are short compared to the characteristic time scales of the evolution.

Self-organised criticality is but one framework which has been proposed to study complex systems. It is defined in analogy with equilibrium critical phenomena. In this context, however, one has a non-equilibrium system that evolves into a state characterised by fluctuations on all length scales and long-range correlations embodied in power-law correlations.

Bak, Tang and Wiesenfeld [5] considered a model representing a dynamically driven, non-equilibrium open system that exhibits behaviour similar to critical phase transitions. It must be noted that the model does not represent all dynamically driven systems, but only captures the essence of some with threshold dynamics. Locally, at each position in space, the dynamic variable (energy, stress, etc.) or its derivatives have a maximum allowed value. When this maximum is exceeded, because of external perturbations, the system responds by redistributing, say, energy to surrounding positions. As an explicit example consider a pile of sand on a flat table. The dynamic variable in this case is the height of the sand column at a point and its derivative is the local slope of the pile. When the local slope exceeds a certain value, because of an external agent adding sand, the pile responds by redistributing sand to neighbouring positions by means of avalanches, in an attempt to restore the slope to below its maximum value.

Bak et al. [5] observed that the model evolves to a state where fluctuations occur on all length scales as is seen from the power-law event size distribution for avalanches. It was suggested that the power-law distributions are a manifestation of some underlying long-range correlation

between the microscopic degrees of freedom of the model and thus of a system at a critical point.

Beyond this point the analogy with equilibrium critical phenomena breaks down in that, unlike the situation in equilibrium systems, there seem to be no external parameters such as temperature or pressure that have to be tuned explicitly to special values to observe the critical behaviour. Hence the name self-organised criticality.

An important feature of systems that exhibit SOC behaviour is the separation of time scales [2]. The relaxation events occur on a time scale much shorter than the time required for the local dynamic variables to reach their threshold value. In practise this is equivalent to saying that there are no external perturbations during relaxation events.

The sandpile model on the flat table is a good example of a complex system consisting of many degrees of freedom that evolve to a state where their collective behaviour starts playing a crucial role. The final state of the system depends in detail on the local state of each part of the pile and its interaction with the neighbouring sites.

1.5 Examples of SOC systems

In this section we briefly consider a few real systems that have been investigated as possible examples of systems exhibiting SOC.

1.5.1 Earthquakes

Earthquakes occur due to the relative motion of tectonic plates along faults in the crust of the earth [2]. Because of friction between the plates, they are prevented from moving relative to each other in a smooth manner. The plates stick together until the stress at the interface exceeds the friction between them. Once this happens, the plates slip.

The phenomenon described above has some of the features of a SOC system. Clearly the stress at the interface between the plates is the dynamic variable with a threshold value equal to the friction between the plates. Earthquakes thus have threshold dynamics. The relative motion of the tectonic plates, which occurs on a scale of a few centimeters per year, serves as the slow driving force. The process of accumulating stress occurs over many years, while the release thereof happens in a few seconds. There is thus clearly a separation of time scales.

When the plates slide relative to each other, seismic waves are radiated. The size of an earthquake is characterised by the amount of energy E released by these seismic waves. The distribution of earthquake sizes is found to be a power law $P(E) \sim E^{-B}$. This is known as the Gutenberg-Richter law for earthquake sizes. The exponent B shows some geographical dependence, but usually falls in the interval 1.8 to 2.2.

Another quantity of interest is the temporal frequency of aftershocks following a large earthquake. It also follows a power-law $n(t) \sim t^{-A}$, where $n(t)$ is the number of aftershocks occuring a time t after a major earthquake. This relation for the aftershocks is known as Omori's law. The exponent A has values lying between 1 and 1.5.

Even though the earthquake sizes have a broad distribution, there appears to be a maximum size that earthquakes can have. This maximum size is determined by the thickness of the layer of the earth's crust. This is an example of a finite-size effect which will be discussed in Chapter 2. The power-law distribution is thus relevant up to a certain scale after which system size has to be compensated for.

1.5.2 Sandpiles

Since the introduction of the concept of SOC, and Bak, Tang and Wiesenfeld's use of the sandpile as an intuitive example of a system exhibiting SOC behaviour, a reasonable amount of experimental work [9, 10, 11] has been performed on real sandpiles to verify if it does exhibit SOC behaviour.

In one experiment [9] avalanches were induced in the sandpile by sprinkling sand grains onto the pile. However, a narrow distribution of avalanche lifetimes was found with no sign of power-law behaviour or criticality. The dynamics of the sandpile is such that the angle of the slope of the pile oscillates between two extreme values, θ_r, the angle of repose and θ_m, the maximum slope. As the system is perturbed θ increases until it reaches θ_m. An avalanche then occurs and it lasts till θ is lowered to θ_r again.

In another series of experiments [10, 11] on real sandpiles power-law behaviour was observed. In [10] and [11] a sandpile on a circular base, mounted on a scale was studied. Small avalanches were found to exhibit power-law behaviour. Avalanches containing between 3 and 80 grains are distributed as $P(s) \sim s^{-2.5}$, where s is the mass carried out of the system by the avalanche. When the diameter of the base is increased the power-law behaviour is lost and system-spanning avalanches dominate the dynamics. The system thus does not display true SOC behaviour.

1.5.3 Ricepiles

The appearance of a characteristic event size in the real sandpile seems to be due to inertial effects. As the grains move down the slope, they gain kinetic energy and become difficult to stop. Rice grains have a smaller mass density than sand grains and one thus expects inertial effects to be less important.

In ref.[12] a series of experiments was performed on three types of rice that differed in surface quality and aspect ratio (length divided by width). Type A was unpolished and elongated with

aspect ratio 3.8. Type B was polished with an aspect ratio of 2.0 and type C was polished with an aspect ratio of 2.6.

The rice pile was formed by placing grains between two glass plates that were separated by a distance of about 80 percent of the grain length. Grains were added at a slow rate at one closed edge and allowed to leave the system at the other edge which was open.

The elongated grains were found to move in more or less coherent clusters and their dynamics seem to be dominated by local friction. The rounded grains of type B were found to be very difficult to stop once they were moving.

From the redistribution of mass during an avalanche the gravitational energy released was calculated. This release of gravitational energy was used as a measure of the avalanche size. For type A and type C rice the avalanche distribution was $P(E) \sim E^{-\alpha}$ with $\alpha \sim 2.04$. The distribution of energy released does not change with increasing system size.

Rice of type B was observed to have a size distribution that falls off like a stretched exponential $P(E) \sim \exp\{-(E/E_0)^{\gamma}\}$. The systems with elongated grains thus seem to exhibit SOC behaviour while those with rounded grains do not. This seems to be consistent with the idea that the existence of local thresholds is an important ingredient for SOC behaviour to be observed. Because the rounded grains flow so easily down the slope, it eliminates threshold dynamics.

1.5.4 Other examples of possible SOC systems

Here we briefly list a few more real systems that are believed to exhibit SOC behaviour. It is believed that the formation of landscapes and landslides occurs through a SOC process. In observations of landslides in the Himalayas, Noever [13] observed that the avalanche sizes, measured by the volume of sand involved in a slide, are distributed according to a power-law. In a series of controlled laboratory experiments on the formation of landscapes, Somfai et al. [14] also observed that the avalanches leading to the formation of landscapes are power-law distributed.

It is also believed that the fluctuations in economics, such as price changes, are due to a self-organising mechanism. In the 1960's Mandelbrot [15] investigated the price changes of various commodities and observed that these price changes also had a broad distribution.

Whether these systems are really poised at some critical point, remains to be verified. However, based on observations thus far it seems as if SOC is a useful framework within which one can explain these phenomena. In the next chapter we discuss a simple cellular automaton, the sandpile model, that has become the standard test-bed for studying SOC.

CHAPTER 2
Sandpile Models

2.1 Introduction

In the previous chapter we introduced the concept of self-organised criticality. In the present chapter we consider the BTW sandpile model, originally introduced by Bak, Tang and Wiesenfeld [5], as a paradigm for studying SOC. We start by defining the model and then discuss its statistical properties. Following this, we discuss the derivation of simple scaling relations for the various distribution exponents. We conclude the chapter by briefly mentioning variants of the BTW sandpile model.

2.2 The BTW Sandpile Model

The model is defined on a d-dimensional lattice. Each lattice site i is assigned an integer value z_i, which indicates the height of a sand column at that position. The evolution of the model is defined in terms of two operations: (a) random addition of particles, and (b) relaxation events.

(a) At each time step a site is selected at random and the height there is increased by one unit. That is,

$$z_i \to z_i + 1. \tag{2.1}$$

(b) If z_i exceeds some specified threshold value, z_c (also called the critical height), the site topples by discarding particles to its nearest neighbours. That is, if $z_i > z_c$

$$z_i \to z_i - 2d, \tag{2.2}$$

$$z_j \to z_j + 1, \tag{2.3}$$

where the $j's$ are the nearest neighbours of the site i. If any of the neighbouring sites are unstable, i.e. $z_j > z_c$, they will also topple, giving rise to an avalanche of such toppling events. The avalanche ends when all sites are stable, i.e $z_i \leq z_c$, for all i. We assume here that z_c is the same for all lattice sites. All lattice sites that are unstable at a given time step are toppled simultaneously. While an avalanche is taking place, no particles are added from the outside, implicitly introducing a separation of time scales to the model.

The model is defined so that there is conservation of particles in the bulk of the lattice. We assume the lattice to have open boundaries, therefore particles can leave the system once they

reach the boundaries.

In the following example we illustrate the toppling rules. Consider a 5×5 lattice, and assume the system has evolved into the following stable configuration. We choose the critical height to be 4.

2	3	1	3	4
3	4	3	4	1
2	3	4	4	3
4	2	4	3	2
1	3	3	2	3

Now we continue the evolution by adding a particle to a randomly chosen site. In this case the central site was chosen. It now has height 5 and is unstable and we allow it to topple.

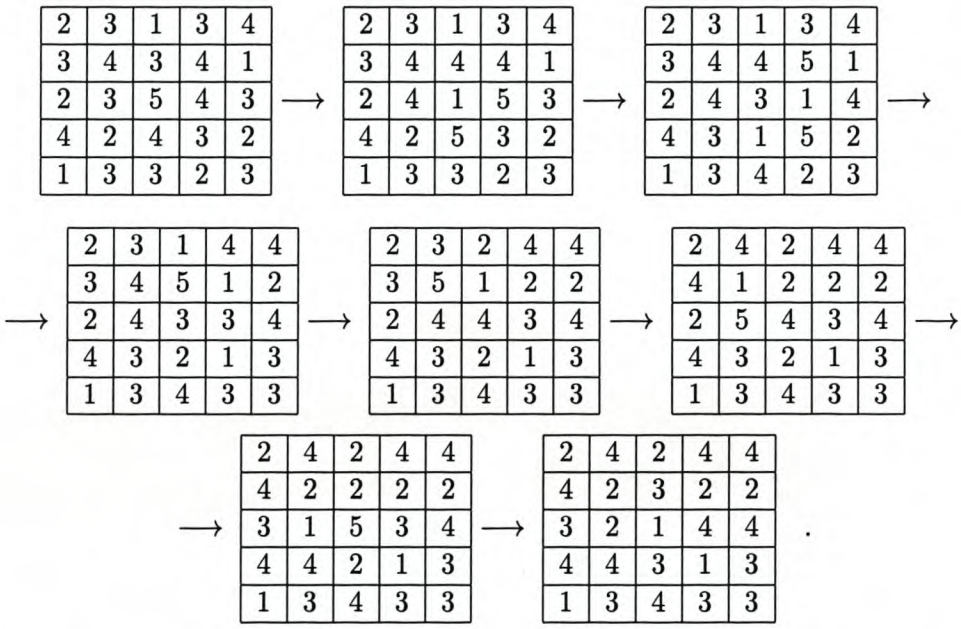

Figure 2.1: Illustration of the toppling rules for the BTW model on a 5×5 lattice

Using the toppling rules defined above, the system evolves into the final configuration shown in the figure.

We are interested in the statistical properties of the system [2]. After sufficient time, the statistical properties of the system are independent of the initial configuration. The system is said to be in a statistically stationary state, i.e. the statistical quantities do not evolve with time. A check of whether the system is in a stationary state is to measure the average height

$\langle z(t) \rangle$ as a function of time, where the average is taken over all lattice sites. Starting from an empty lattice, $\langle z(t) \rangle$ will increase until it fluctuates about an average given by

$$\langle z \rangle = \lim_{T \to \infty} \frac{1}{T} \int_0^T \langle z(t) \rangle dt. \tag{2.4}$$

Once this happens the system is said to be in a stationary state. The physical meaning of a constant $\langle z(t) \rangle$ is that on average the number of particles added to the system equals the number of particles lost at the boundaries, a signal of a statistically stationary state.

2.3 Measurable Quantities

The sandpile responds to external perturbations by means of avalanches. We need to quantify the response of the system. Some useful measures of the response are the lattice area affected by the avalanche, number of topplings and the duration of the avalanche.

The area, a, is the number of sites in the lattice that toppled at least once during an avalanche. The number of topplings s is the total number of relaxation events induced by adding a single particle to the system. In general $s \geq a$ since any site may topple more than once. The duration, t, is defined as the number of simultaneous updates needed to reach a stable configuration. In the example of the previous section the avalanche consisted of 9 topplings events, covered 8 sites and lasted for 7 updates.

2.4 Scaling Relations

Define $p(x)$ as the probability density function for the variable x, with $x \in \{a, s, t\}$. Then, $p(x)dx$ is the probability that x has a value in the interval dx around x. From numerical simulations [2, 5, 16] of the model it is found that in the stationary state, the probability density functions defined above are power-laws,

$$p(s) \sim s^{-\tau}, \tag{2.5}$$

$$p(a) \sim a^{-\lambda}, \tag{2.6}$$

$$p(t) \sim t^{-\alpha}. \tag{2.7}$$

As mentioned in chapter 1, these power-laws are considered to be a manifestation of a system at a critical point and therefore of scale invariance. It was noted by Bak et al. [5] that in the one dimensional case the model did not show critical behaviour. Figure 2.2 shows the cumulative distribution of the toppling number for the 2-dimensional BTW model. We see that it is indeed

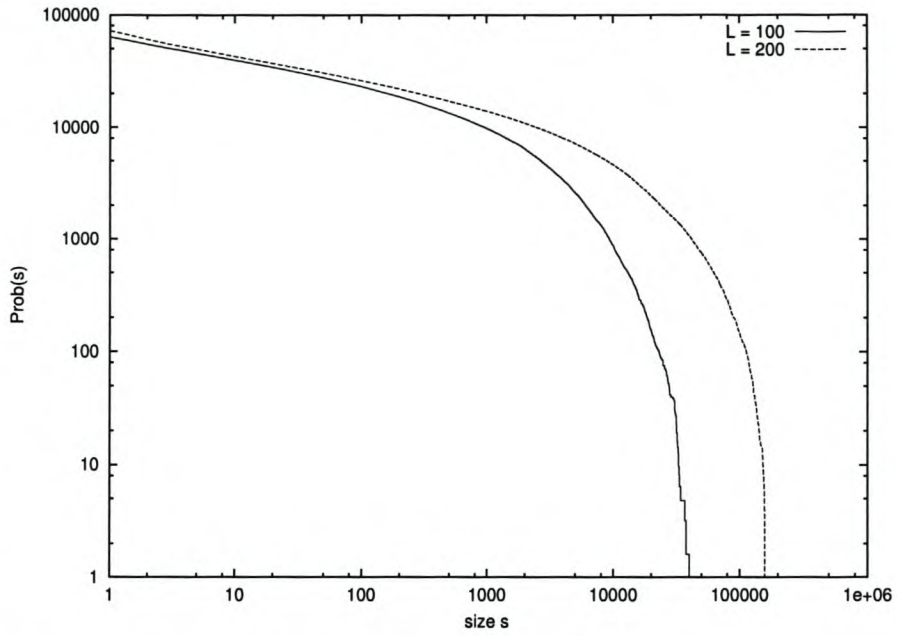

Figure 2.2: The cumulative probability $Prob(s)$ that an avalanche is of size greater than or equal to s, as a function of s for lattice sizes $L = 100$ and $L = 200$.

distributed according to a power-law. For the remainder of this dissertation we will only consider 2-dimensional sandpile models.

The model defined above has all the properties of a SOC system. It has threshold dynamics, a separation of time scales and a stationary state characterised by power-law probability distributions.

Since each of the quantities a, s and t gives a measure of the size of an avalanche, one expects that they will not be independent of each other [2, 17]. Using these relations among the measurable quantities we can derive certain scaling relations between the various distribution exponents [2].

Since there is no characteristic scale in the system, we assume that the area, toppling number and duration are also related to each other through power-law equations. The scaling relations between the measurable quantities are defined in terms of conditional expectation values. Conditional expectation values are defined as follows; the average value of variable x, given that variable y has the value $y = Y$ is given by

$$E[x|y = Y] = \sum_X XP(x = X|y = Y), \tag{2.8}$$

where $P(x = X|y = Y)$ is the conditional probability that variable x has the value X given that

y has value Y. Consider, for example, the subset of avalanches whose area is exactly A. We can now, for example, consider how the average number of topplings S depends on the value of A. In order to fully describe the model, we have to consider the following conditional expectation values:

$$E[s|t=T] \sim T^{\gamma_1}, \tag{2.9}$$

$$E[t|s=S] \sim S^{\frac{1}{\gamma_1}}, \tag{2.10}$$

$$E[s|a=A] \sim A^{\gamma_2}, \tag{2.11}$$

$$E[a|s=S] \sim S^{\frac{1}{\gamma_2}}, \tag{2.12}$$

$$E[t|a=A] \sim A^{\gamma_3}, \tag{2.13}$$

$$E[a|t=T] \sim T^{\frac{1}{\gamma_3}}. \tag{2.14}$$

In the definitions above, we have assumed that there exist some reciprocal relationships between these quantities. We have assumed that they are related as

$$t = s^{\frac{1}{\gamma_1}}, \tag{2.15}$$

$$a = s^{\frac{1}{\gamma_2}}, \tag{2.16}$$

$$a = t^{\frac{1}{\gamma_3}}. \tag{2.17}$$

If this is true, the exponents γ_i are related by

$$\gamma_2 = \gamma_1\gamma_3. \tag{2.18}$$

This can be seen by substituting eq.(2.15) into eq.(2.17);

$$\begin{aligned} a &= (s^{\frac{1}{\gamma_1}})^{\frac{1}{\gamma_3}} \\ &= s^{\frac{1}{\gamma_1\gamma_3}}. \end{aligned} \tag{2.19}$$

Now using eq.(2.16), we have

$$s^{\frac{1}{\gamma_2}} = s^{\frac{1}{\gamma_1\gamma_3}}. \tag{2.20}$$

The relations (2.15) to (2.17) are not strictly true. There might be more than one toppling with the same area. However, we assume that the conditional probabilities have sufficiently narrow support so that one can for example talk of a characteristic number of topplings S for an avalanche of duration T.

We can now construct a set of scaling relations between the exponents by using the following identity for any three stochastic variables x, y and z [17];

$$\int E[x|y = Y]p(y = Y)dY = \int E[x|z = Z]p(z = Z)dZ. \tag{2.21}$$

In eq.(2.21) the identity follows from the fact that the LHS and RHS are both equal to the average value of variable X for a given process. By setting $x = s$, $y = t$ and $z = a$ and assuming that the relations (2.5) to (2.7) hold, we have the folowing;

$$\int E[s|t = T]P(t = T)dT = \int E[s|a = A]P(a = A)dA \tag{2.22}$$

$$\int T^{\gamma_1 - \alpha}dT = \int A^{\gamma_2 - \lambda}dA \tag{2.23}$$

$$T^{\gamma_1 - \alpha + 1} = A^{\gamma_2 - \lambda + 1}, \tag{2.24}$$

following from indefinite integration and where we have dropped the constants.

Using (2.17) we have

$$T^{\gamma_1 - \alpha + 1} = (T^{\frac{1}{\gamma_3}})^{\gamma_2 - \lambda + 1}. \tag{2.25}$$

Thus

$$\gamma_1 - \alpha + 1 = \frac{\gamma_2 - \lambda + 1}{\gamma_3} \tag{2.26}$$

$$\alpha = 1 + \gamma_1 + \frac{\lambda - \gamma_2 - 1}{\gamma_3}. \tag{2.27}$$

Following the same procedure but setting $x = a$, $y = s$ and $z = t$ we derive

$$\tau = 1 + \frac{1}{\gamma_1} + \frac{\lambda - \gamma_3 - 1}{\gamma_2}. \tag{2.28}$$

Now using (2.18), eq.(2.27) can be reduced as follows.

$$\begin{aligned} \alpha &= 1 + \gamma_1 + \frac{\lambda - \gamma_2 - 1}{\gamma_3} \\ &= 1 + \gamma_1 + \frac{\lambda - 1}{\gamma_3} - \frac{\gamma_2}{\gamma_3} \\ &= 1 + \gamma_1 + \frac{\lambda - 1}{\gamma_3} - \gamma_1. \end{aligned} \tag{2.29}$$

Thus,

$$\alpha = 1 + \frac{\lambda - 1}{\gamma_3}. \tag{2.30}$$

Avalanche distributions	Conditional Expectation relations	Assumed power-law scaling
$p(s) \sim s^{-\tau}$ $p(t) \sim t^{-\alpha}$	$E[s\|t=T] \sim T^{\gamma_1}$ $E[t\|s=S] \sim S^{\frac{1}{\gamma_1}}$	$t = s^{\frac{1}{\gamma_1}}$
$p(s) \sim s^{-\tau}$ $p(a) \sim a^{-\lambda}$	$E[s\|a=A] \sim A^{\gamma_2}$ $E[a\|s=S] \sim S^{\frac{1}{\gamma_2}}$	$a = s^{\frac{1}{\gamma_2}}$
$p(t) \sim t^{-\alpha}$ $p(a) \sim a^{-\lambda}$	$E[t\|a=A] \sim A^{\gamma_3}$ $E[a\|t=T] \sim T^{\frac{1}{\gamma_3}}$	$a = t^{\frac{1}{\gamma_3}}$

Table 2.1: Summary of the probability distributions and the corresponding conditional expectation values from which the scaling relations are derived

In a similar way we can reduce (2.28) to

$$\tau = 1 + \frac{\lambda - 1}{\gamma_2}. \tag{2.31}$$

By introducing the conditional expectation values for the measurable quantites and assuming that they scale as power-laws of each other we have been able to derive simple scaling relations for the various distribution exponents. See Table 2.1 for summary of the relation between the various probability density functions in terms of conditional probabilities.

2.5 Finite-Size Scaling

Due to the finite size of the systems considered, the power-law probability distributions will only be valid up to some cut-off size [2, 18, 19]. It is assumed that this cut-off scales with the system size as $x_c \sim L^{\nu}$ so that in the thermodynamic limit the cut-off diverges. The probability distribution will thus be of the following form,

$$p(x) \sim x^{-\tau_x} g\left(\frac{x}{x_c}\right), \tag{2.32}$$

where g is a scaling function correcting for the finite system size. The scaling function $g(\frac{x}{x_c})$ should have the property $g(0) = 1$, so that in the thermodynamic limit the distribution is just a pure power-law as expected. Let us denote $p(x, L)$ as the probability distribution for variable $x \in \{a, s, t\}$ in a system of linear size L. The finite-size scaling ansatz is

$$p(x, L) = L^{-\beta_x} g\left(\frac{x}{L^{\nu_x}}\right). \tag{2.33}$$

By inserting the identity $\left(\frac{x}{L^{\nu_x}}\right)^{-\frac{\beta_x}{\nu_x}} \left(\frac{x}{L^{\nu_x}}\right)^{\frac{\beta_x}{\nu_x}}$ into (2.33) we can rewrite the finite-size scaling ansatz in a form where the x dependence of the probability density is clear and the L-dependence

has been absorbed in the scaling function. That is

$$\begin{aligned} p(x,L) &= L^{-\beta_x} g\Big(\frac{x}{L^{\nu_x}}\Big) \\ &= L^{-\beta_x}\Big(\frac{x}{L^{\nu_x}}\Big)^{-\frac{\beta_x}{\nu_x}}\Big(\frac{x}{L^{\nu_x}}\Big)^{\frac{\beta_x}{\nu_x}} g\Big(\frac{x}{L^{\nu_x}}\Big) \\ &= x^{-\frac{\beta_x}{\nu_x}}\tilde{g}\Big(\frac{x}{L^{\nu_x}}\Big), \end{aligned} \tag{2.34}$$

where,

$$\tilde{g}\Big(\frac{x}{L^{\nu_x}}\Big) = \Big(\frac{x}{L^{\nu_x}}\Big)^{\frac{\beta_x}{\nu_x}} g\Big(\frac{x}{L^{\nu_x}}\Big). \tag{2.35}$$

Comparing eqs. (2.32) and (2.34) we have another scaling relation,

$$\tau_x = \frac{\beta_x}{\nu_x}. \tag{2.36}$$

By making use of the fact that the average size of the avalanche $\langle s\rangle$ scales with the system size as

$$\langle s\rangle \sim L^2, \tag{2.37}$$

[20, 19, 18] we can derive further relations between the finite size scaling exponents.

$$\begin{aligned} \langle s\rangle &= \frac{\int_1^\infty sP(s,L)ds}{\int_1^\infty P(s,L)ds} \\ &= \int_1^\infty sL^{-\beta} g\Big(\frac{s}{L^\nu}\Big)ds \end{aligned} \tag{2.38}$$

Set $x = \frac{s}{L^\nu}$ where x is now a rescaled variable. Then we have that if $s = 1$ then $x = \frac{1}{L_\nu}$ and if $s = \infty$ then $x = \infty$. Thus the integral becomes

$$\begin{aligned} \langle s\rangle &= \int_{\frac{1}{L^\nu}}^\infty L^{2\nu-\beta} x g(x)dx \\ &= L^{2\nu-\beta}\int_{\frac{1}{L^\nu}}^\infty x g(x)dx \\ &\simeq L^{2\nu-\beta}, \end{aligned} \tag{2.39}$$

where it is assumed that the integral converges [18, 19]. Thus we have the scaling relation

$$2\nu - \beta = 2. \tag{2.40}$$

We see that apart from providing the corrections to scaling of the probability distributions

due to the finite size of the system, the finite size scaling ansatz also provides us with useful scaling relations between the exponents of the model. We shall return to the finite size scaling ansatz in chapter 3 when we consider the structure of avalanches in more detail.

2.6 Other Sandpile Models

The BTW model discussed in this chapter is the prototype for models of SOC. Since its introduction numerous versions of the sandpile model have been proposed to identify the relevant parameters of the model. In this section we shall briefly mention these models and how they relate to the BTW model. However, for the rest of this work we shall concentrate on the BTW model since it has certain features, to be discussed in the next chapter, that makes it simpler to treat analytically and numerically.

2.6.1 Directed Model

This model [21] is defined similarly to the BTW model, but it has a preferred direction of toppling. When a site, labelled by coordinates (x, y), becomes unstable it only distributes particles to two adjacent neighbours *eg.* the sites $(x+1, y)$ and $(x, y-1)$. The choice of transfer direction is made at the start of the simulation and remains fixed for the duration of the simulation. Thus particles are transferred along a preferred direction. This model has been solved exactly by Dhar and Ramaswamy [21] in all dimensions. The avalanche distributions also display power-law behaviour. For the two-dimensional case, the distribution exponents have the values $\tau = 2.33$ and $\alpha = \frac{3}{2}$. For the directed model the area and toppling number are the same since each site can only topple once during an avalanche.

2.6.2 Zhang Model

The evolution rules for this model [22] are defined almost exactly like that of the BTW model. The only difference is that the dynamical variable at each site can now take on continuous values. It is more intuitive to think of these dynamical variables as energy instead of the height of the sand column at that a site. Without loss of generality one can set the threshold value $E_c = 1$.

The probability distribution for event sizes and durations also show power-law behaviour. From numerical simulations one finds that the exponents for toppling number, area and duration are respectively $\tau = 1.282 \pm 0.01$, $\lambda = 1.338 \pm 0.015$ and $\alpha = 1.512 \pm 0.014$.

2.6.3 Manna Model

This model [23] is defined so that each site can have a maximum of one particle. Just as in the BTW model a site is chosen at random and a particle is added there. If the site is

already occupied, it becomes unstable and topples. Upon toppling its height decreases to zero and it discards both particles to neighbours that are chosen randomly. The model is thus not deterministic, unlike the previous models.

The probability distribution for number of topplings and duration also satisfy power-law behaviour with exponents $\tau = 1.28 \pm 0.02$ and $\alpha = 1.47 \pm 0.10$ respectively.

The BTW sandpile model has, in a certain sense, become for SOC what the Ising model is for equilibrium critical phenomena. Although the model is simply defined, very few questions can be answered exactly and most of the results for the model are based on numerical simulations. For example, the distribution exponents have not been calculated exactly. However, Dhar and coworkers have been able to compute some of the properties of the model analytically using an algebraic approach. In the next chapter we discuss the basic formalism they have developed and some of the results that have followed from their work.

CHAPTER 3
Abelian Sandpiles

3.1 Introduction

In this chapter we consider some of the properties of the sandpile model in more detail. We start by formulating the model more generally in terms of a toppling matrix and addition operators. Using the toppling matrix, we show that the addition operators commute. This property is later used to decompose the avalanche process into more elementary sub-processes. Next, we define recurrent configurations in terms of the addition operators and introduce a simple test, called the burning algorithm, to see if a given configuration is recurrent or not. We also calculate some stationary state correlation functions of the model and find that they can be expressed in terms of the toppling matrix.

In the latter half of the chapter we use the burning algorithm to show the equivalence between recurrent sandpile configurations and one-rooted spanning trees. This equivalence then allows us to use graph-theoretical techniques to compute certain properties of the sandpile model.

3.2 Definition

We summarise the evolution rules again. Consider the square lattice with sites labelled by indices $i = 1, 2, ..., N$. At each site the height of the sand column is given by an integer value z_i. The evolution rules are [20]

1. At each time step a site is selected, with a probability p_i and the height increased by one unit,
$$z_i \to z_i + 1. \tag{3.1}$$

2. The toppling rule is now given in terms of the toppling matrix. If $z_i > z_{i,c}$ then
$$z_j \to z_j - \Delta_{ij} \text{ for every } j. \tag{3.2}$$

Without loss of generality we can set $z_{i,c} = \Delta_{ii}$. The toppling matrix has the following properties.

1. $\Delta_{ii} > 0$ for every i. This condition ensures that the height of a site decreases upon toppling. Δ_{ii} is the number of particles removed from site i when it topples.

2. $\Delta_{ij} \leq 0$ for $i \neq j$. This ensures that heights of nearest neighbours increase when a site topples. Δ_{ij} is the number of particles passed to j when i topples.

3. $\sum_j \Delta_{ij} \geq 0$ for every i. This condition determines the amount of sand lost from the system during a toppling event. For bulk toppling $\sum_j \Delta_{ij} = 0$ and only for boundary topplings is it greater than zero.

We shall restrict ourselves to the special case where the Δ matrix is symmetric. As a specific example consider a 2×2 lattice, with the site labels indicated,

1	2
3	4

.

The Δ matrix has the following entries:

$$\Delta_{ij} = \begin{cases} 4 & \text{if } i = j \\ -1 & \text{if i and j are nearest neighbours} \\ 0 & \text{otherwise.} \end{cases}$$

Therefore, we have

$$\Delta = \begin{pmatrix} 4 & -1 & -1 & 0 \\ -1 & 4 & 0 & -1 \\ -1 & 0 & 4 & -1 \\ 0 & -1 & -1 & 4 \end{pmatrix} \tag{3.3}$$

3.3 Abelian property

Let us denote a stable configuration by C. Define operators a_i [20] such that the stable configuration $C' = a_i C$ is obtained after adding a particle at site i and allowing the system to relax. We shall prove that for all i and j the operators satisfy the following property:

$$a_i a_j C = a_j a_i C \tag{3.4}$$

i.e. the operators commute. Physically this means that the final configuration does not depend on the order in which unstable sites are relaxed.

This can be proven as follows. Suppose we have a configuration with two unstable sites i and j. Toppling i first increases the height of j (using the condition 2 for the toppling matrix), but the site j remains unstable. Next topple site j. Because of these two toppling events, the height at any other site, say k, changes by $-\Delta_{ik} - \Delta_{jk}$. The nett change in height at site k is clearly independent of the order in which the sites i and j were toppled. By repeated use of this argument we can show that this applies to any number of unstable sites. Together with this we

also have that the operations of toppling an unstable site i and adding a particle to a site j, commute. This is so because if site i is unstable it will topple whether or not the particle was added to j first. It is clear that the Abelian property of toppling events holds even when the Δ matrix is asymmetric.

3.4 Recurrent Configurations

It can be shown that the sandpile model dynamics is Markovian [20, 24]. From the general theory of Markov chains it is known that the stable configurations can be divided into two classes namely transient and recurrent. In terms of the addition operators, a recurrent configuration is defined as follows. A configuration is said to be recurrent if and only if there exist positive integers m_i $(i = 1, 2, \ldots, N)$ such that

$$a_i^{m_i} C = C. \tag{3.5}$$

Using the Abelian property we find that if C is a recurrent configuration, then $a_j C$ (for all j) is also recurrent. This follows since

$$a_i^{m_i}(a_j C) = a_j a_i^{m_i} C = a_j C. \tag{3.6}$$

Denote by R the set of all recurrent configurations. From eq.(3.6) we have that R is closed under multiplication by the operators a_i. Thus, once the system gets into the set of recurrent configurations it cannot escape from there again. In the stationary state the transient configurations appear with zero probability. The long-time behaviour of the system is thus determined by its evolution from one recurrent configuration to another.

If we consider only the recurrent configurations, we can define inverses for the addition operators as follows;

$$a_i^{-1} C = a_i^{m_i - 1} C. \tag{3.7}$$

We can now use these inverses of the addition operators to compute the probability for having a recurrent configuration. Let $P(C, t)$ denote the probability of having the system in the configuration C at time t. Further, let $W(C \to C')$ denote the probability that the system changes from configuration C to C'. Then we can write the master equation for the probability distribution $P(C, t)$ as

$$P(C, t+1) = P(C, t) - \sum_{C' \in R} P(C, t) W(C \to C') + \sum_{C' \in R} P(C', t) W(C' \to C). \tag{3.8}$$

The transitions in the system occur as a result of the action of the operators a_i on the stable configurations. The transition probabilities can be written as

$$W(C \to C') = \sum_{i=1}^{N} p_i \tilde{P}(a_i C = C'), \tag{3.9}$$

where p_i is the probability that site i is chosen as the random addition position and $\tilde{P}(a_i C = C')$ is the probability that the system evolves from C into C' when a particle is added to site i. Now using the invertibilty of the operators a_i we can write

$$\tilde{P}(a_i C = C') = \begin{cases} 1 & \text{if } C = a_i^{-1} C' \\ 0 & \text{otherwise.} \end{cases}$$

If we now substitute eq.(3.9) into the master equation and use eq.(3.4) we have

$$P(C, t+1) = P(C,t) - \sum_{C' \in R} P(C,t) \sum_{i=1}^{N} p_i \tilde{P}(a_i C = C') + \sum_{C' \in R} P(C',t) \sum_{i=1}^{N} p_i \tilde{P}(a_i C' = C) \tag{3.10}$$

Summing over the configurations C' we have

$$P(C, t+1) = P(C,t) - \sum_{i=1}^{N} p_i P(a_i C, t) + \sum_{i=1}^{N} p_i P(a_i^{-1} C, t). \tag{3.11}$$

From this equation it follows that a time-independent uniform distribution, $P(C,t) = constant$ is a stationary solution to the master equation [2]. Thus all recurrent configurations appear with equal probability, $\frac{1}{|R|}$, where $|R|$ is the number of recurrent configurations.

Since it is only the recurrent configurations that are of interest in the stationary state we have to be able to characterise them. Before we show how to test whether a configuration is recurrent or transient we first introduce the concept of forbidden subconfigurations (FSC). There are some subconfigurations of the sandpile that cannot be reached by the addition and relaxation rules unless they are present initially.

A forbidden subconfiguration is a set of connected sites F such that the height, z_i of each site in F is less than or equal to the number of neighbours of site i in the set F. Mathematically it is expressed by the following inequality

$$z_j \leq \sum_i (-\Delta_{ij}) \text{ for every } j \in F. \tag{3.12}$$

Consider the following examples;

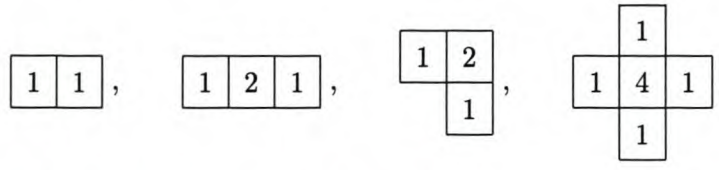

Consider for example the first subconfiguration in the list above. Because $z_i > 0$ a height of 1 in the steady state can only be created if one of the sites toppled. A toppling at any other site can only make the height of either of these sites greater than 1. But toppling at either of these sites would result in a height of 2 for the other one. Thus, a configuration with two adjacent sites having the minimum height is not allowed. We can now extend this argument to prove that the other subconfigurations shown are also forbidden.

3.4.1 The Burning algorithm

There exists a simple test [20, 25], called the burning algorithm, to test whether a given configuration is recurrent or transient. Consider a stable configuration. Initially all sites are considered unburnt. A site can burn if and only if its height is strictly greater than its number of unburnt neighbours. The process is repeated until no more sites can burn. If all the sites burn, the initial configuration was recurrent. If some of the sites remain unburnt, the original configuration was transient and the unburnt sites form a FSC. Consider the following example of using the burning algorithm to test if the configuration is recurrent or not. We see that the

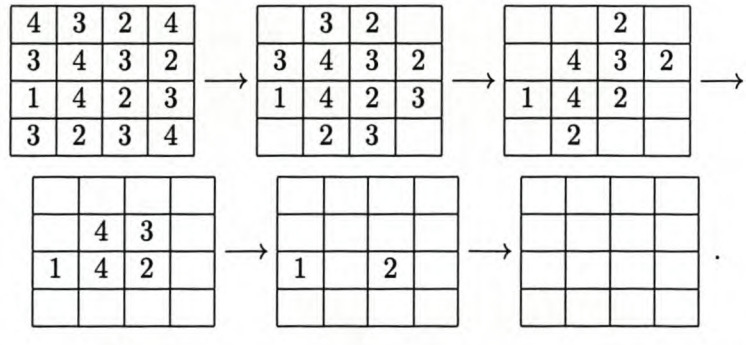

Figure 3.1: An example of using the burning algorithm

lattice burned completely, therefore the configuration is recurrent.

3.5 Number of recurrent configurations

In the previous section we showed that the configurations of the ASM can be divided into two classes namely recurrent and transient. Now we use the toppling matrix to calculate the number

of recurrent configurations of the model in the steady state [2, 20].

Let us first introduce some notation. Let $\hat{e}_i$, $(i = 1, 2, \ldots, N)$ be the unit vectors in the space Z^N. We can denote any configuration of the model as $\vec{z} = \sum_{i=1}^{N} z_i \hat{e}_i$, where z_i is the height at site i.

We can define an equivalence relation on the set of all configurations. Two configurations are said to be equivalent if they evolve into the same configuration when toppled. To give this a more precise mathematical definition we define toppling operators, T_n that have the following effect on a configuration $C = \{z_i\}$.

$$T_n\{z_i\} = \begin{cases} \{z_i - \Delta_{ni}\} & \text{if } z_n > \Delta_{nn} \\ \{z_i\} & \text{otherwise.} \end{cases}$$

Thus, two configurations are said to be equivalent if there exist sequences such that

$$T_{n_1} T_{n_2} \ldots T_{n_m} \vec{z} = T_{\tilde{n}_1} T_{\tilde{n}_2} \ldots T_{\tilde{n}_{\tilde{m}}} \tilde{\vec{z}}. \tag{3.13}$$

Using eq.(3.5) this becomes

$$z_j - \Delta_{n_m j} - \Delta_{n_{m-1} j} - \ldots \Delta_{n_1 j} = \tilde{z}_j - \Delta_{\tilde{n}_{\tilde{m}} j} - \Delta_{\tilde{n}_{\tilde{m}-1} j} - \ldots \Delta_{\tilde{n}_1 j} \tag{3.14}$$

$$z_j - \sum_{i=1}^{m} \Delta_{a_i j} = \tilde{z}_j - \sum_{i=1}^{\tilde{m}} \Delta_{\tilde{a}_i j}. \tag{3.15}$$

This can be rewritten in the form

$$\tilde{z}_j = z_j - \sum_{i=1}^{N} r_i \Delta_{ij}, \tag{3.16}$$

where the r_i indicate how many times site i toppled. This equation says that two configurations are equivalent if the one can be obtained from the other by a series of toppling events.

Let $\vec{n}_i = \sum_{j=1}^{N} \Delta_{ij} \hat{e}_j$. Define the space V by

$$V \equiv span\{\vec{n}_1, \vec{n}_2, \ldots, \vec{n}_N\} = \{\vec{v} \in Z^N | \vec{v} = \sum_{i=1}^{N} \alpha_i \vec{n}_i, \alpha_i \in Z^N\} \tag{3.17}$$

We now show that the set of equivalent configurations is in the space V. Any configuration of the model can be written as

$$\vec{z} = z_1 \hat{e}_1 + z_2 \hat{e}_2 + \ldots + z_N \hat{e}_N. \tag{3.18}$$

In this form eq.(3.16) is

$$\begin{aligned}
\tilde{\vec{z}} &= (z_1 - \sum_{i=1}^{N} r_i\Delta_{i1})\hat{e}_1 + (z_2 - \sum_{i=1}^{N} r_i\Delta_{i2})\hat{e}_2 + \ldots + (z_N - \sum_{i=1}^{N} r_i\Delta_{iN})\hat{e}_N \\
&= (z_1\hat{e}_1 + z_2\hat{e}_2 + \ldots + z_N\hat{e}_N) + \Big\{\sum_{i=1}^{N}(-r_i)\Delta_{i1}\hat{e}_1 + \sum_{i=1}^{N}(-r_i)\Delta_{i2}\hat{e}_2 + \ldots \sum_{i=1}^{N}(-r_i)\Delta_{iN}\hat{e}_N\Big\} \\
&= (z_1\hat{e}_1 + z_2\hat{e}_2 + \ldots + z_N\hat{e}_N) + \sum_{i=1}^{N}(-r_i)\Big\{\Delta_{i1}\hat{e}_1 + \Delta_{i2}\hat{e}_2 + \ldots \Delta_{iN}\hat{e}_N\Big\} \\
&= \vec{z} + \sum_{i=1}^{N}(-r_i)\sum_{j=1}^{N}\Delta_{ij}\hat{e}_j \\
&= \vec{z} + \sum_{i=1}^{N}(-r_i)\vec{n}_i. \qquad (3.19)
\end{aligned}$$

Thus, we see that two configurations are equivalent if and only if $\tilde{\vec{z}} - \vec{z}$ is in the space V. It can be shown that there is exactly one recurrent configuration in each equivalence class. Thus the number of recurrent configurations is equal to the number of equivalence classes. This is simply equal to the volume of V. We know that the volume of V is given by $\det\Delta$. Therefore the number of recurrent configurations is just

$$|R| = \det\Delta. \qquad (3.20)$$

3.6 Two-point correlation function

We now calculate the two-point correlation function for the sandpile model in the stationary state [20]. Let G_{ij} be the average number of toppling events at site j caused by an avalanche initiated at site i. We know that in the steady state, on average, the number of particles added to a site must be equal to the number of particles discarded from that site.

The average number of particles entering a site j is

$$J_{in}(j) = \sum_{i\neq j} G_{ik}(-\Delta_{kj}) + \delta_{ij}, \qquad (3.21)$$

where the second term on the RHS represents the random addition of particles from the outside.

The average number of particles leaving a site j is

$$J_{out}(j) = G_{ij}\Delta_{jj}. \qquad (3.22)$$

Thus using the conservation of particles in the stationary state we have

$$\sum_{i \neq j} G_{ik}(-\Delta_{kj}) + \delta_{ij} = G_{ij}\Delta_{jj} \tag{3.23}$$

$$\sum_{k=1}^{N} G_{ik}\Delta_{kj} = \delta_{ij}. \tag{3.24}$$

From eq.(3.24) we see that G_{ij} is the inverse of the toppling matrix, i.e

$$G_{ij} = \Delta_{ij}^{-1}. \tag{3.25}$$

However, the toppling matrix is just the lattice Laplacian [2]. Therefore eq.(3.24) is the discrete version of the Poisson equation. We know what the solutions to this equation are. In the continuous limit we have,

$$G(r) \sim \begin{cases} r^{2-d} & \text{for } d > 2 \\ \log r & \text{for } d = 2, \end{cases}$$

where r is the distance separating sites i and j and d is the spatial dimension.

We see that the correlation function is also a power-law, further indicating that the sandpile is indeed in a critical state with long range correlations.

3.7 Height correlations

In this section we show how the toppling matrix can be used to calculate the probability that a site has a given height and also the height correlations in the stationary state [25]. We will only outline the procedure and not go through the detailed calculations.

Suppose we want to calculate the probability that a given site, say i, has height 1. This is given by

$$P(z_i = 1) = \frac{\text{no. of recurrent configurations in which } z_i = 1}{\text{total no. of recurrent configurations}}. \tag{3.26}$$

We know that the denominator is simply $\det \Delta$. To calculate the numerator we introduce an auxiliary lattice in which all recurrent configurations have the height of site i equal to 1. We then show that the set of recurrent configurations on the auxiliary lattice is in one-to-one correspondence with those that have $z_i = 1$ on the original lattice.

Consider a configuration, C, with $z_i = 1$. Define the auxiliary lattice such that the bonds between site i and three of its neighbours, say N, S, and W, are deleted. Thus, when i topples it cannot pass particles to these three neighbours. Also, for each bond deleted, we reduce the threshold height of the sites at the end of the bond by 1.

On the auxiliary lattice, now consider the configuration C' obtained from C, on the original lattice, by decreasing the height of each of i's neighbours by one. We can show that the configuration C', on the auxiliary lattice, burns in the same order as C on the original lattice[2]. From this it follows that the recurrent configurations on the auxiliary lattice are in one-to-one correspondence with recurrent configurations on the original lattice with $z_i = 1$. We know that the number of recurrent configurations on the auxiliary lattice is $\det\Delta'$, where Δ' is the toppling matrix on the auxiliary lattice. Δ' is defined as

$$\Delta'_{ij} = \Delta_{ij} + B_{ij}, \tag{3.27}$$

where the $B_{ij} = 0$ except for the following elements.

$$B_{NN} = B_{WW} = B_{SS} = -1 \tag{3.28}$$

$$B_{ii} = -3 \tag{3.29}$$

$$B_{iN} = B_{Ni} = B_{iS} = B_{Si} = B_{iW} = B_{Wi} = 1. \tag{3.30}$$

Thus to solve eq.(3.26) we have to consider the quantity

$$\begin{aligned} P(1) &= \frac{\det\Delta'}{\det\Delta} \\ &= \det(\Delta^{-1})\det(\Delta') \\ &= \det(\Delta^{-1}\Delta') \\ &= \det(\Delta^{-1}(\Delta + \mathrm{B})) \\ &= \det(\mathrm{I} + \Delta^{-1}\mathrm{B}). \end{aligned} \tag{3.31}$$

A computation of (3.31) gives the value of $P(1) = 0.0736$. The distributions for $z_i = 2, 3, 4$ can also be calculated, but require more advanced techniques. Detailed calculations of these give the following results [25]

$$P(2) = 0.1739 \tag{3.32}$$

$$P(3) = 0.3063 \tag{3.33}$$

$$P(4) = 0.4461. \tag{3.34}$$

These values agree very well with numerical estimates for them. Manna [16] calculated these

[2]See appendix A for an example

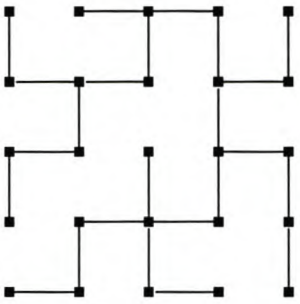

Figure 3.2: A spanning tree on a 5×5 lattice

relative occupation of sites numerically and found

$$P(1) = 0.073 \tag{3.35}$$

$$P(2) = 0.174 \tag{3.36}$$

$$P(3) = 0.307 \tag{3.37}$$

$$P(4) = 0.446. \tag{3.38}$$

Using a similar technique of ratio of determinants one can calculate the joint probability that two sites i and j both have height 1. If r is the distance separating the sites one finds [25]

$$P(z_i = 1, z_j = 1) \sim P^2(1) + \frac{K}{r^4}, \tag{3.39}$$

with K constant. One can also calculate the general case where the sites i and j have heights a and b respectively. It has the form,

$$P(z_i = a, z_j = b) \sim P(a)P(b) + \frac{K_a K_b}{r^4}. \tag{3.40}$$

Once again we see that the correlations in the sandpile are long-ranged. This serves as further evidence that the sandpile is in a critical state. In section 3.4 we introduced the concept of FSC's and saw that there were certain restrictions on the allowed height configurations. It is therefore not surprising that the heights of the sandpile are long-range correlated.

3.8 Equivalence of Recurrent Configurations and Spanning Trees

In this section we show how to use the burning algorithm to construct a spanning tree representation of the recurrent configurations [26]. A spanning tree is defined on a graph as a set of edges that touch all nodes, but contains no loops (see Figure 3.2). It provides a unique

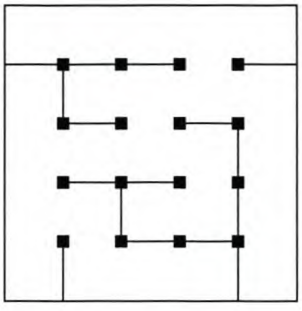

Figure 3.3: The spanning tree representation for the configuration in fig.(3.1)

path between any two nodes on the graph.

To be able to construct the spanning tree representation, we introduce an extra site, called the "sink", that is connected to every boundary site. When using the burning algorithm we can now consider the fire to start at the sink, spread to the boundary and from there to the rest of the lattice.

We have seen that due to the Abelian property the order in which sites are burned is not important. However, we introduce a specific burning order by introducing a so-called burning time. In this formulation the sink is assumed to burn at time $t = 0$ and the boundary sites at time $t = 1$. We define a site to be burnable at time t if its height strictly exceeds its number of unburnt neighbours at time t. A site that is burnable at time t burns at time $t + 1$.

For a site to burn at time t it must have had at least one neighbour that burned at time $t - 1$. The spanning tree for a recurrent configuration is constructed by connecting each site to a neighbour with a burning time one unit less than its own.

However, there can be some ambiguity since two or more neighbours may have a burning time of $t-1$. Let us denote the number of unburnt neighbours of site i by ξ_i and the number of burnt neighbours by K_i. Then we can always write the height of site i as $z_i = \xi_i + K_i$. Now depending on the value of K_i, we construct the unique path between i and its neighbours. Let us introduce an order of preference for the neighbouring sites as follows,

$$N > E > S > W. \tag{3.41}$$

If the height at site i is $z_i = \xi_i + s$ we say the fire reached site i from its s-th neighbour and we choose the s-th neighbour from the ordered list.

Consider the example in Figure 3.3 At time $t = 1$ the four corner sites are burned. Consider the top left site and assign it the label A. The value of $\xi_A = 2$ and $K_A = 2$, since it can be connected to the sink by two bonds. The two possible neighbours from which the fire reached

site A are N and W. According to the ordering introduced we have that $N > W$. Since the height at A is $z_A = \xi_i + 2$ we choose the second neighbour from the ordered list of possible bonds, i.e. W.

As a second example, consider the bottom left site and call it B. For this site $\xi_B = 2$ and $K_B = 1$. The possible neighbours are W and S. In the ordered list we have $S > W$. And since $z_B = \xi_B + 1$ we choose the first neighbour i.e. S.

3.9 Waves of Toppling

We start this section by briefly discussing the problem with the finite-size scaling ansatz for the toppling number proposed in chapter 2. The finite-size scaling ansatz is

$$p(x, L) = x^{-\tau_x} g\left(\frac{x}{L^{\nu_x}}\right), \tag{3.42}$$

where $x \in \{a, s, t\}$. It is found that for the area the scaling form (3.42) works very well, but for the toppling number there are significant deviations from it [27]. Recent simulations indicate that the BTW model may possibly be characterised by multi-fractal behaviour [28]. At first it was thought that avalanches that reach the boundary obey different statistics than bulk avalanches and therefore the observed deviations from the simple scaling form occur. However these deviations also appear for bulk avalanches that do not touch the boundary. To illustrate that there is indeed a problem with the scaling for the toppling number, the ratio $\frac{P_s(x,L)}{P_a(x,L)}$ of the integrated distributions $P_s(x, L) = \int_x^\infty p_s(x', L)dx'$ was considered in ref [27]. If the area and the toppling number obey the same scaling form then we expect the ratio to scale as $x^{\tau_a - \tau_s}$ for $x << min\{L^{\nu_a}, L^{\nu_s}\}$.

From numerical simulations it is found that this ratio does not scale as expected [27]. A possible explanation for the deviation from the simple scaling is that in the BTW model sites can perform multiple topplings during an avalanche. This would explain why the deviation is seen for bulk topplings as well and not just because of some boundary effects.

In this section we show how an avalanche can be decomposed into more elementary objects, called waves of toppling. From the definitions of waves it follows that each site can only topple once in a wave. We find that waves obey the simple finite size scaling ansatz of eq.(3.42).

The other reason for decomposing an avalanche into waves follows from the fact that we can construct a spanning tree representation of waves of toppling in a similar way that we did for recurrent configurations. We can then use results from graph theory to make predictions about the statistics of waves.

3.9.1 Definition of waves of toppling

From the Abelian property of the BTW model we know that the order in which unstable sites are toppled is not important. The wave decomposition performs the toppling of sites in a very specific order [29]. Suppose we add a particle at site i and it becomes unstable. We allow the site to topple and if it becomes unstable a second time, we prevent it from toppling again, first allowing all other sites that became unstable due to its first toppling to relax. This set of relaxation events constitutes the first wave of topplings. Once all sites are stable, we allow the initial site to topple a second time and repeat the process. This forms the second wave of topplings. This process is repeated until the initial site is stable and the avalanche comes to an end.

We now prove that in a wave each site only topples once. Consider a site j_1 that initially topples before a neighbouring site j_2. In order for site j_2 to topple twice, the site j_1 has to topple a second time. If j_1 is constrained to topple once then j_2 can also only topple once. Therefore, since the initial site of the avalanche is constrained to topple once during a wave, and all other sites topple after it, all sites involved in the wave can only topple once.

Because of this property of waves, avalanches initiated at the boundary consist of only one wave. For a site to become unstable a second time all four its neighbours have to topple when it is initially relaxed. Since a boundary site has a maximum of three neighbours, it cannot topple a second time.

The size of the wave is the area covered by the wave. Denote the size of the i-th wave by w_i. The size of the avalanche is then simply the sum of the sizes of all the waves, i.e.

$$s = w_1 + w_2 + \ldots + w_N, \tag{3.43}$$

if the avalanche consists of N waves.

3.10 Waves and Spanning Trees

In this section we show how to obtain a spanning tree representation of waves by once again using the burning algorithm [29, 27]. We will construct a spanning tree representation for unstable configurations that appear after successive waves during an avalanche.

To do this we introduce an auxiliary model on a new lattice. In the new model we add a bond between the sink and the site i where an avalanche is initiated. The site i is now on the boundary of the new lattice. Therefore, every avalanche starting at i will consist of exactly one wave. In fact each avalanche in the new model corresponds exactly to a wave in the original model.

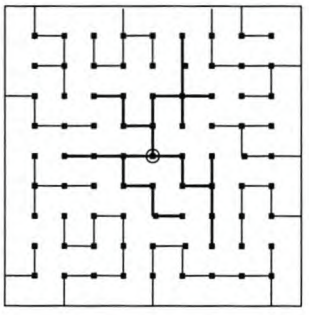

Figure 3.4: Example of a two-root spanning tree showing the wave decomposition of avalanches

We can now apply the burning algorithm to this new lattice to obtain its spanning tree representation. Upon burning we find that some branches of the tree are completely independent of site i, but one branch passes from the sink to i and the fire then propagates further from there.

If we now remove the bond between site i and the sink, we obtain two disjoint subtrees. The one containing site i corresponds to the sites toppled during the wave and those not containing i to those sites that were not toppled. The lattice is now spanned by a two-rooted tree, whereas for the stable recurrent configurations it is spanned by a one-rooted tree (see Figure 3.4).

3.11 Wave distributions using spanning trees

The spanning tree representation of waves allows us to compute some statistical properties of waves using graph-theoretical techniques. We start by calculating the distribution for the size of the last wave in an avalanche. We note that an avalanche ends when the initial site is on the boundary of the wave since it then only has a maximum of three neighbours that can topple. Manna et al. [30] showed that obtaining the spanning tree representation for the last wave is equivalent to cutting a random bond with the site where the bond was cut on the perimeter of one of the resulting sub-trees. The size of the last wave is the number of sites disconnected from the tree by cutting the bond. They found that the distribution for the number of sites removed from the tree when deleting a random bond is

$$P(s) \sim s^{-\frac{11}{8}}. \tag{3.44}$$

From this we can now calculate the probability distribution for general waves. To do this we consider the evolution of the sandpile as a sequence of waves, without considering to which avalanche they belong. We know that the waves are in one-to-one correspondence with all recurrent configurations on the auxiliary lattice and that recurrent configurations appear with

equal probability in the steady state. Thus all waves occur with equal probability in the steady state. However, the last wave of each avalanche differs from the general wave in terms of the location of the origin of the wave. For general waves the origin can be anywhere in the bulk, whereas for the last wave it is on the boundary. Therefore we have to consider a correction to the distribution for waves, induced by the last wave. If we denote the perimeter of the wave by l then the probability per site for being the origin of the last wave is $\frac{P_{last}(s)}{l}$. If s is the size of the wave, there are s possibilities. Therefore the probability for all waves has to be multiplied by the factor $\frac{sP_{last}(s)}{l}$ [29]. Using the relation $l \sim s^{\frac{5}{8}}$ [30] we have the probability distribution for all waves is

$$P_{all}(s) \sim \frac{sP_{last}(s)}{l} \tag{3.45}$$

$$= \frac{sP_{last}(s)}{s^{\frac{5}{8}}} \tag{3.46}$$

$$= \frac{1}{s}. \tag{3.47}$$

This result agrees very well with numerical simulations. Even though this result is relatively easy to obtain, it has proven more difficult to obtain the avalanche distribution from it. There have been attempts to obtain the avalanche distribution from the wave distribution but these have not been successful.

This chapter discussed some advances in our understanding of the BTW sandpile model. Even though all the relevant quantities have not been calculated thus far, the existence of the elegant operator formalism and the results it produces does make one hopeful that the model may indeed be solved completely analytically. The wave picture of avalanches further helps to give insight into our understanding of the avalanche phenomenon.

3.12 Application of Abelian Sandpile results

In the following chapter we discuss the connection between sandpile models and mining induced seismicity. In motivating our approach, we find that the results that follow from the analyis of the model based on Dhar's abelian formalism are qualitatively similar to that observed in the more traditional approaches to modelling induced seismicity. Also, indirect observations of the conditions of the earth's crust would suggest that SOC is indeed a suitable formalism with which to study mining induced seismicity.

CHAPTER 4
Mining Induced Seismicity and SOC

4.1 Introduction

In Chapter 1 we briefly discussed the study of tectonic earthquake phenomena using Self-Organised Criticality as the framework of investigation. In the present chapter we look to extend the analysis to the case of seismicity induced by human activity by establishing a correspondence between mining-induced seismicity and the sandpile model. We start by considering the general equilibrium conditions that exist in the earth's crust prior to any perturbations. Then we briefly mention examples of induced seismicity. Next we look at the common features of the sandpile model and mining-induced seismicity and give a motivation for this approach to modelling mining-induced seismicity.

4.2 Equilibrium conditions in the earth's crust

In general it can be accepted that the rock mass in the earth's crust is in equilibrium under the action of virgin or primitive stresses [31]. These primitive stresses are the natural stresses in the rock mass prior to any perturbations. The virgin stresses at a point in the rock mass are the result of events in the geological history of the rock mass and may be the result of many earlier stress states. We now briefly discuss three contributions to the virgin stress in the rock mass.

Consider a geologically undisturbed rock mass. The vertical component of the virgin stress is a result of the effect of gravity on the rock mass [31]. In homogeneous rock the vertical component is simply the pressure exerted by the weight of a column of overlying rock of unit cross sectional area. If the rock density is ρ and taking the origin at the surface and letting z increase vertically downward, the vertical component of the primitive stress is

$$\sigma_z = \rho g z, \tag{4.1}$$

where g is the gravitational acceleration and z the depth below surface.

The horizontal components of the virgin stress also depend on the depth below surface. For a relatively undisturbed rock mass the two horizontal components are generally found to be equal, $\sigma_x = \sigma_y$ [31, 32]. They usually take the form

$$\sigma_x = \sigma_y = k\sigma_z, \tag{4.2}$$

where k is a constant that depends on the geographical location. Values of k are generally between 0.5 and 1.0, but in some places values of k exceeding 1.0 have been measured. The origin of this may be in tectonic stresses or residual stresses in the rock mass.

Tectonic stresses arise due to the straining of the crust, either currently or in previous times [31]. These stresses may be due to regional uplift, faulting, folding or surface irregularities. The superposition of tectonic stresses on gravity induced stresses can result in significant changes in both the magnitude and direction of the resultant virgin stresses. Furthermore, regional uplift may develop horizontal tensile stresses, causing the formation of faults. Faults divide the rock mass into distinct blocks and thus disrupt the continuity of the stress field [31, 33].

Residual stresses are defined as stresses that remain in the rock mass even after their cause is removed [31]. It is usually explained as follows. During the history of the rock mass it may have been been subjected to higher stresses than it is at present. When removing the load causing the stress, the relaxation of the rock is inhibited. Thus, part of the earlier stress remains locked in the rock. One can consider it as a memory effect.

4.3 Examples of induced seismicity

In this section we briefly describe examples of induced seismicity without giving a detailed account of the mechanisms. The first example is that of the changes in pore pressure that occur due to reservoir impoundment [34]. The pore pressure below a reservoir changes due to the change in water level of the reservoir and subsequently induces fracturing, or increases the stress on existing faults causing them to slip. This is easily understood since there is now a greater gravitational load on the rock mass beneath the reservoir. The most common values of the stress changes induced by reservoir filling are between 1 and 2 MPa. These stress changes are enough to induce seismic events of magnitude ≥ 2.5 in areas that are historically seismically inactive. However, there are also reported cases where stress changes of 0.1 MPa, corresponding to small changes in the water level, were sufficient to induce seismicity in historically seismically inactive areas [34].

The second, related, source of induced seismicity is that of hydrocarbon extraction. Again, relatively small stress changes can induce seismic activity in previously seismically inactive areas [34].

4.3.1 Mining-induced seismicity

The third example of induced seismicity is the one of central importance in this dissertation, i.e., seismicity induced by deep-level gold mining in South Africa.

Before we discuss mining-induced seismicity we briefly describe the mechanism by which earthquakes occur in tectonic settings where the driving force is the mantle motion. The mechanism described here is also applied to mining-induced seismicity. We also discuss how earthquake sizes are determined. Earthquakes occur on fault planes or discontinuities in the earth's crust. Due to the motion of the mantle, the tectonic plates move relative to one another. However, due to friction, the plates do not slide over each other smoothly. As long as the frictional forces exceed the driving forces, the plates will not slip, but only build up potential energy and deform each other elastically. Once the driving force exceeds the frictional force, the two plates move very suddenly relative to each other. This sudden slip motion induces elastic waves that travel through the crust and this is what is experienced as the ground motion associated with earthquakes. These seismic waves are recorded at monitoring stations and the amplitude, frequency and energy of these seismic waves contain information about what happened at the source of the earthquake.

There are various measures of earthquake sizes. The two we will discuss are the energy radiated by the seismic waves and a quantity called the seismic moment. We first discuss energy budget on a fault plane during an earthquake. Some of the energy is used to overcome the frictional forces opposing slip. Once the slip motion starts, friction is not "turned off", so there is work required to overcome it. Secondly, some of the energy is expended on the fracturing of rock as the plates slide. The rest of the energy is radiated as seismic waves. We see that what is measured as the energy of the earthquake is only a portion of the total energy available on the fault plane.

Seismic moment is a measure of the slip that takes place when the earthquake occurs. It is defined by the relation

$$M_o = \mu A d, \tag{4.3}$$

where μ is the rigidity of the rock mass, A is the area of the slip and d is distance over which the plates slipped. Seismologists have ways of determining A and d from seismograms and other geodetic data and μ is a property of the rock mass that is generally known, so M_o can be determined [35].

Another important quantity is the ratio of radiated energy to the seismic moment. That is

$$\sigma_A = \frac{E_r}{M_o} = \frac{E_r}{\mu A d}. \tag{4.4}$$

This ratio is known as the apparent stress and it is a measure of the change in stress at the source of the earthquake [36, 35].

We now turn to the discussion of mining-induced seismicity in deep-level gold mining in

South Africa. Ore deposits in South African gold mines are generally found at depths that vary between 1000m and 3500m. In order to extract the ore, deep excavations have to be made. These excavations include the initial work for the development of the infrastructure to operate the mine. This includes sinking the shaft for travelling up and down the mine, transport roadways underground, etc. For the discussion here and for all practical purposes we suppose that the rock mass including the development infrastructure is in equilibrium. The process of extracting the ore on a daily basis for production purposes is considered the driving mechanism of the system. The ore is extracted by placing explosive charges in the reef and removing the first 1.5m of rock by detonating the explosives. In the gold-mining industry this is known as "blasting". The explosion and subsequent removal of the rock mass serves as the perturbation on the equilibrium stress conditions and subsequently induce both elastic and inelastic deformation in the rock mass surrounding the excavations [36].

As we have already mentioned above, the same mechanism for earthquakes described above holds in the context of seismicity induced by mining activities. In a typical mine there are already existing fault planes on which the stress state is perturbed by the mining process. However, in addition to existing natural faults, the mining excavations can also create further planes of weakness on which slip can take place.

It is interesting to note that in the gold mining industry seismic activity is strongly correlated with production activity. There is ample data showing the decrease in seismic activity on week-ends and other days when no production takes place [34, 36]. Thus, it is reasonable to assume that the seismic activity is due to human ativities that perturb the stress state of the rock mass.

It is important to note that not all perturbations induce seismic activity. There is evidence of stress changes due to hydrocarbon extraction and reservoir filling with no subsequent seismicity in the area of interest [34].

The essential point to grasp is that prior to a perturbation equilibrium stress conditions exist in the rock mass. The perturbation can cause some locations to deform inelastically during the redistribution of stress to re-establish equilibrium. This is similar to the situation for the sandpile model. Prior to any external perturbations, the system is stable (equilibrium) and no activity takes place. Once an external perturbation is applied, and some sites become unstable, there is an internal redistribution of sand to reach a stable configuration again.

4.4 The Gutenberg-Richter relation

In Chapter 1 we briefly mentioned the Gutenberg-Richter law for earthquakes and its power-law form that led to speculation that seismicity is a self-organised critical phenomenon. It may

not be entirely obvious how the form presented in Chapter 1 is related to the usual form seen in seismicity or earthquake physics literature. In this section we explicitly show the connection and also clarify how the Gutenberg-Richter relation enters into our correspondence between seismicity and the sandpile model.

The Gutenberg-Richter law states that the number of earthquakes equal to or greater than magnitude m_E is given by

$$\log_{10} N_{\geq m_E} = a_E - b_E m_E, \tag{4.5}$$

where a_E is a constant with some geographical dependence and b_E is the so-called b-value of the distribution. The subscript E denotes the fact that we are considering the radiated seismic energy during an earthquake. The magnitude m_E is defined as

$$\log_{10} E = K + \beta m_E, \tag{4.6}$$

which gives

$$m_E = \frac{1}{\beta} \log_{10} E - \frac{K}{\beta}, \tag{4.7}$$

with β and K constants. The magnitude here is the familiar Richter scale magnitude that is used to quantify the size of an earthquake. Combining eqs. (4.5) and (4.7) we find

$$\log_{10} N_{\geq m_E} = a_E - b_E(\frac{1}{\beta} \log_{10} E - \frac{K}{\beta}) \tag{4.8}$$

$$= a_E + \frac{b_E K}{\beta} - \frac{b_E}{\beta} \log_{10} E. \tag{4.9}$$

This in turn gives

$$N_{\geq}(E) \sim E^{-B}, \tag{4.10}$$

with $B = \frac{b_E}{\beta}$ and where the $\geq$ sign indicates that we are dealing with the cumulative distribution. This is the form which was mentioned in Chapter 1.

As we saw in the previous section, seismic events are also characterised by their seismic moment which is a measure of the deformation at the source of the event. The Gutenberg-Richter relation in terms of moment then becomes

$$\log_{10} N_{\geq m_M} = a_M - b_M m_M, \tag{4.11}$$

with m_M the moment-magnitude which is defined by [36]

$$m_M = \frac{2}{3}\log_{10} M_o - 6.1. \tag{4.12}$$

This is known as the Hanks-Kanamori moment-magnitude relation. Combining (4.11) and (4.12), exactly like we did for the case of radiated energy, we find a power-law form for the Gutenberg-Richter law in terms of the seismic moment

$$N_{\geq}(M_o) \sim M_o^{-\alpha}, \tag{4.13}$$

where $\alpha = \frac{2}{3}b_M$.

The Gutenberg-Richter law is a cumulative distribution of events equal to or greater than some given size. The sandpile model event size distributions discussed in Chapter 2 are non-cumulative distribution functions of the form $p(x) \sim x^{-\lambda}$. However, the cumulative probability distribution functions for these distributions are of the form

$$P_{\geq}(x) \sim \frac{1}{1-\lambda}x^{1-\lambda}, \tag{4.14}$$

which is also a power-law [37]. It is from the fact that both self-organised criticality and seismic systems have power-law cumulative distributions that the initial attempts to describe seismicity in terms of an SOC framework are motivated.

We just make a few comments here concerning cumulative and non-cumulative distribution functions. In essence when one cumulates the probability distribution function you are binning the data, which automatically smooths it. Hence the observed scatter in Figure 4.1 and the smooth curve in Figure 4.2. We should also point out that the apparent multi-valuedness of the distribution function in Figure 4.1 is simply due to the scale on which it is viewed. If one were to view the distribution on a scale that zooms in sufficiently, it will indeed be clear that it is single-valued.

Finally we comment on the usefulness of the Gutenberg-Richter relation in the mining seismicity context. In the mining industry the calculation of seismic hazard is of crucial importance. Seismic hazard is simply a generic term used to quantify the probability of having potentially dangerous situations underground in a mine. This includes large magitude events, rock falls, etc. The Gutenberg-Richter relation is used in many of these calculations of seismic hazard. For example, the mean recurrence time for events greater than a certain magnitude, $T_r(\geq m_M)$, is

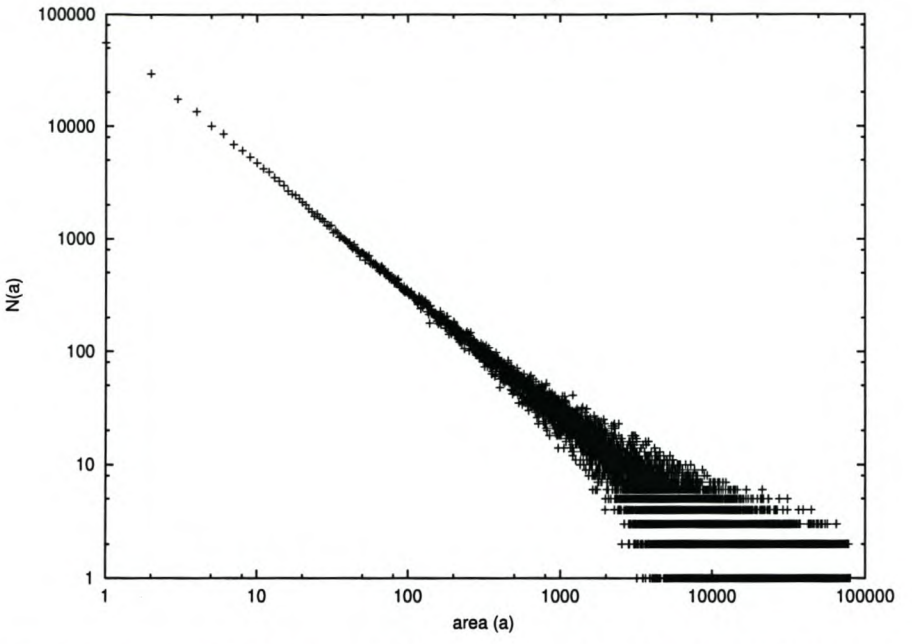

Figure 4.1: The non-cumulative event size distribution for the BTW sandpile model.

computed using the following relation [38]

$$T_r(\geq m_M) = \frac{\Delta t}{N(\geq m_M)}, \tag{4.15}$$

where Δt is the period of observation and $N(\geq m_M)$ is obtained from eq.(4.11).

4.5 Correspondence between the sandpile models and mining-induced seismicity

In the previous two sections we gave examples illustrating how induced seismicity relates to self-organised criticality. In this section we summarise all that and also discuss some of the shortcomings of the sandpile model approach to modelling seismicity. We first give a list of similarities between seismicity and general self-organised critical systems,

- both are complex systems with a large number of degrees of freedom;
- both posses inherent randomness;
- their major statistical ingredients are scale invariant over several orders of magnitude;
- they both have hierarchially organised structures;
- both phenomena are intermittent in space and time;

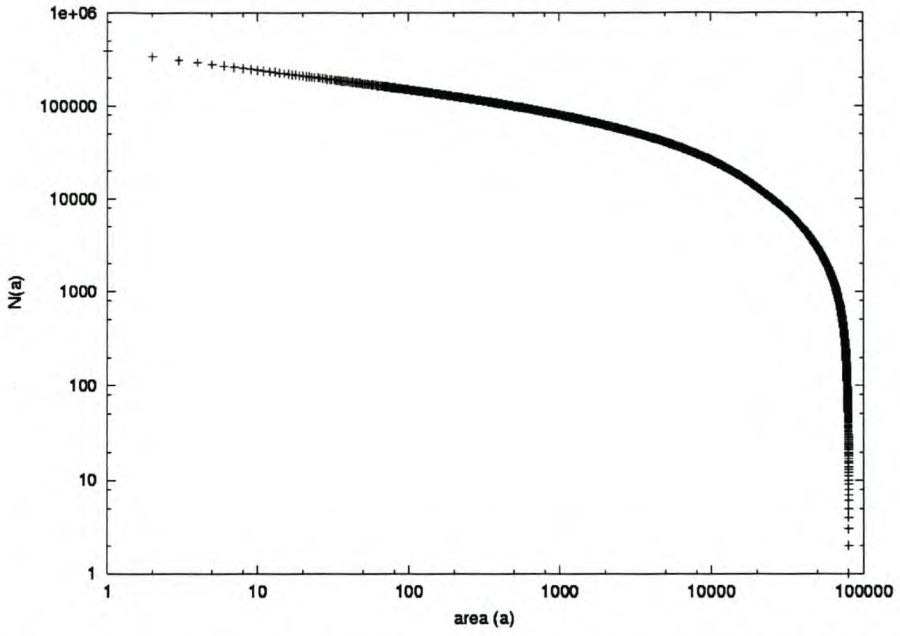

Figure 4.2: The cumulative event size distribution for the BTW sandpile model.

- both phenomena are subject to threshold dynamics.

In order to apply the sandpile model of self-organised criticality to induced seismicity we make the following correspondences. The sandpile lattice configuration represents some stress state of the rock mass while particle addition corresponds to increasing the stress load on the rock mass. Finally avalanches will be representative of the hierarchical failure once the rock mass reaches its failure threshold under the load added by the external perturbation.

It is tempting, but misleading, to think of the sandpile lattice of possible cracks as a physical volume of rock. A more appropriate picture, however, may be to think of the lattice as a simplification, where the physical rock mass has been subtracted out, leaving one free to concentrate on the potential fractures, stress transfer and hierarchical cascades of stress transfer without a specific spatial connection. The lattice can be viewed as a so-called "fracture space". Of course, we then lose sight of the fact that fractures surround excavations.

It is also important to mention some of the apparent shortcomings of the sandpile model approach to modelling mining-induced seismicity. The sandpile model, by construction, cannot take real-time into consideration. Time steps correspond to the moments when perturbations are applied. Since avalanches have different durations, the real-time intervals between external perturbations will not be constant. In the mining situation, however, external perturbations are applied at fixed real times. This does not present a problem since for all practical applications the rock mass is assumed to have reached equilibrium before the next external perturbation is

applied. There will thus be no activity unless an external perturbation is applied. In a sense the "time steps" in the mining context are also set by the external perturbations.

Although the sandpile model is a very simple toy model we have seen that it captures the essential aspects of mining-induced seismicity phenomena. In the following chapter we investigate further similarities between the sandpile model and seismicity and enquire if the sandpile has any predictive qualities.

4.6 Bi-modal distributions

At this point we briefly discuss another observed feature of mining-induced seismicity and its possible realisation in terms of the sandpile model. It is observed in mining-induced seismic data that sometimes the Gutenberg-Richter relation has two distinct slopes [38]. Here we briefly describe a possible explanation for this observed two-slope or bi-modal phenomenon. We also discuss how such behaviour may be generated in the sandpile model.

4.6.1 Bi-modal distributions in mining-induced seismic data

The explanation for the two-slope behaviour is due to Jordan and Richardson and collaborators [39]. Based on extensive monitoring of mining-induced sesimic events in major South African gold mines, they have concluded that there are two types of mining-induced seismic events, designated as type A and type B.

Type A events are clustered around development ends and show an upper cutoff is size of $M \sim 0.5$. Based on the seismograms, they interpret these events to be "fracture-dominated" ruptures of competent rock, induced by dynamic stress during blasting.

Type B events are spatially and temporally distributed throughout the active mining area. Again, based on interpretations of seismograms these events are said to be "friction-dominated" ruptures that occur on existing faults or other geologic structures. Type B events also have a minimum cutoff of about $M \sim 0.0$.

4.6.2 Bi-modal distributions in the BTW sandpile model

We now briefly discuss how such bi-modal behaviour can be generated in the BTW sandpile model. At the outset we point out that the aim is simply to show that one can construct a model that can reproduce such bi-modal behaviour. We are not in any way trying to explain the fundamental reasons for such bi-modal behaviour.

The simplest way to understand the Jordan-Richardson explanation is that there are two mechanisms, fracture and slip, operating somewhat independently of each other and that they give rise to different values for the slope of the Gutenberg-Richter relation.

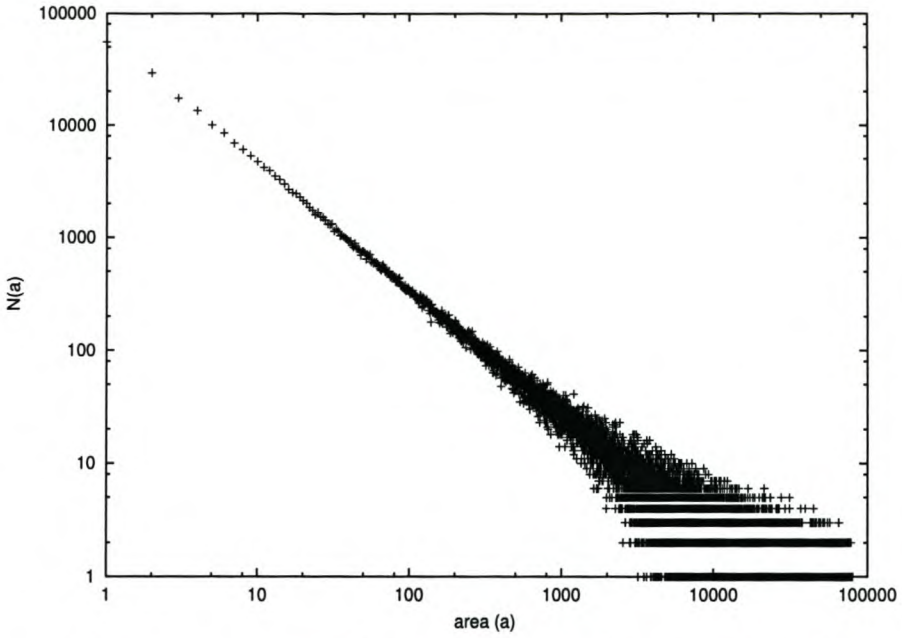

Figure 4.3: The probability distribution with $p = 0.0$

We incorporate this in the sandpile model by introducing two different types of toppling rules. The simplest combination is that of non-directed (BTW model) and directed toppling rules (see section 2.6.1 for the definition of directed toppling). One starts with an ordinary non-directed BTW model and then superimposes directed toppling with a given probability. We introduce a continuously varying parameter p that ranges from 0 to 1. $p = 0$ corresponds to non-directed toppling and $p = 1$ to directed toppling. At each time step a random number α with $0 < \alpha < 1$ is generated. If $\alpha < p$ the directed toppling rule is applied and if $\alpha \geq p$ the non-directed toppling rule is followed.

In Figures 4.3 to 4.7 we plot the event size distribution for a range of p-values. For $p = 0$ (normal BTW model) and $p = 1.0$ (directed model) we find the expected power-law behaviour of the event size distribution. For $p = 0.5$, which effectively simulates that directed and non-directed topplings are equally likely, the event size distribution is a deviation from the simple power-law. There is a slight "kink" which is reminiscent of the two-slope Gutenberg-Richter law. We thus see when we have two toppling rules superimposed on each other, the sandpile model also exhibits a form of bi-modality. It should be mentioned, however, that the bi-modal behaviour in the sandpile model is not as pronounced as in real seismic data. It is not clear why this is the case.

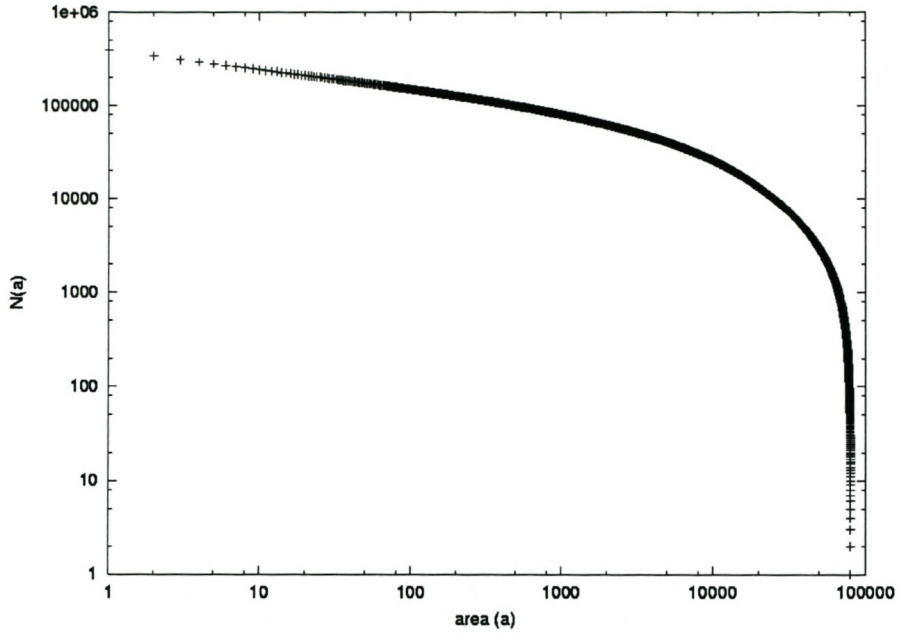

Figure 4.4: The cumulative probability distribution with $p = 0.0$

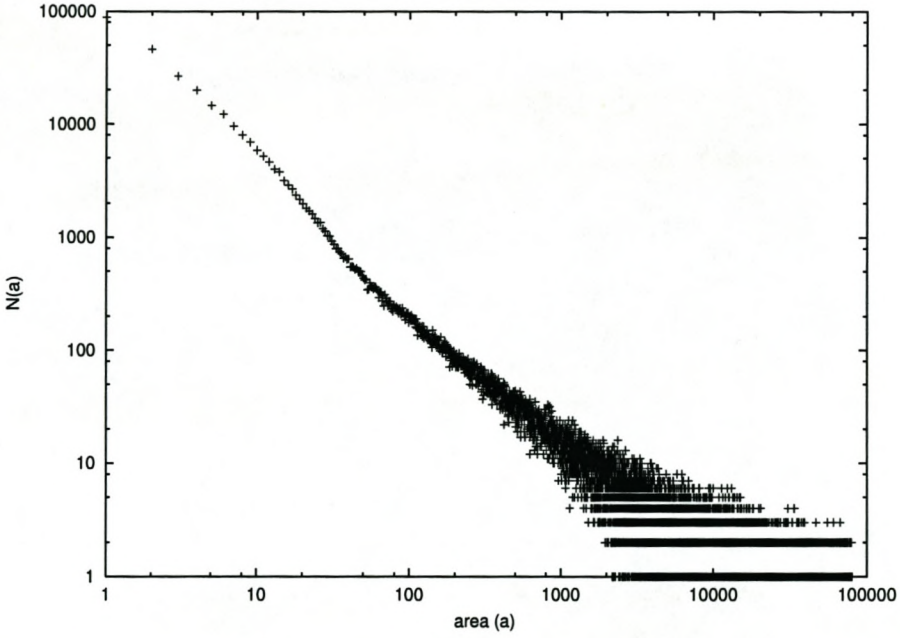

Figure 4.5: The probability distribution with $p = 0.5$.

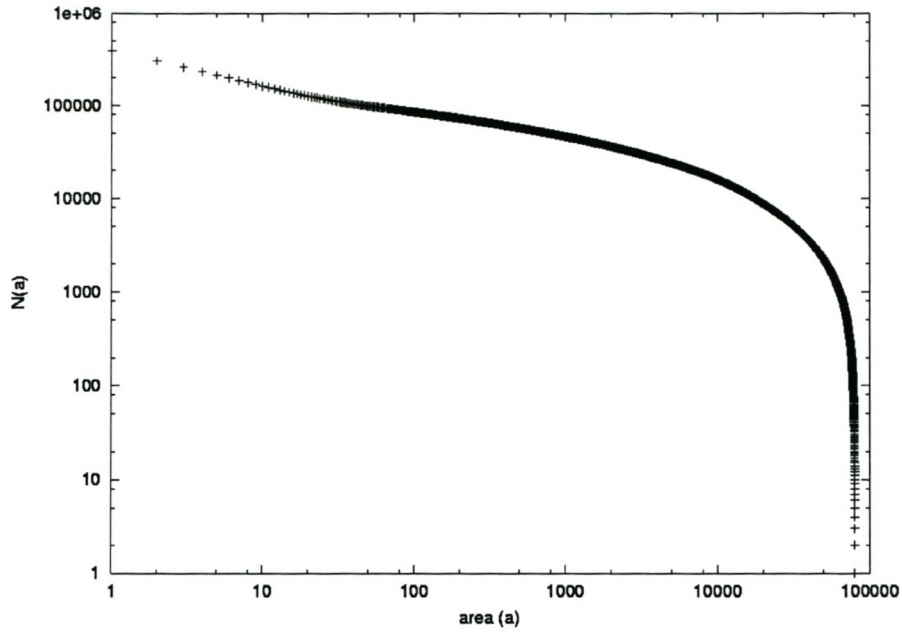

Figure 4.6: The cumulative probability distribution with $p = 0.5$.

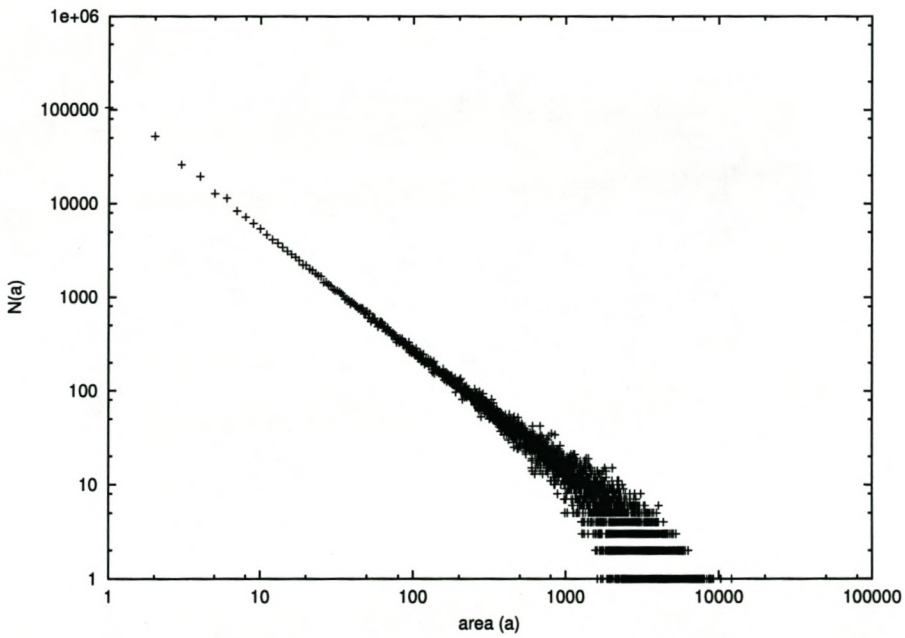

Figure 4.7: The probability distribution with $p = 1.0$.

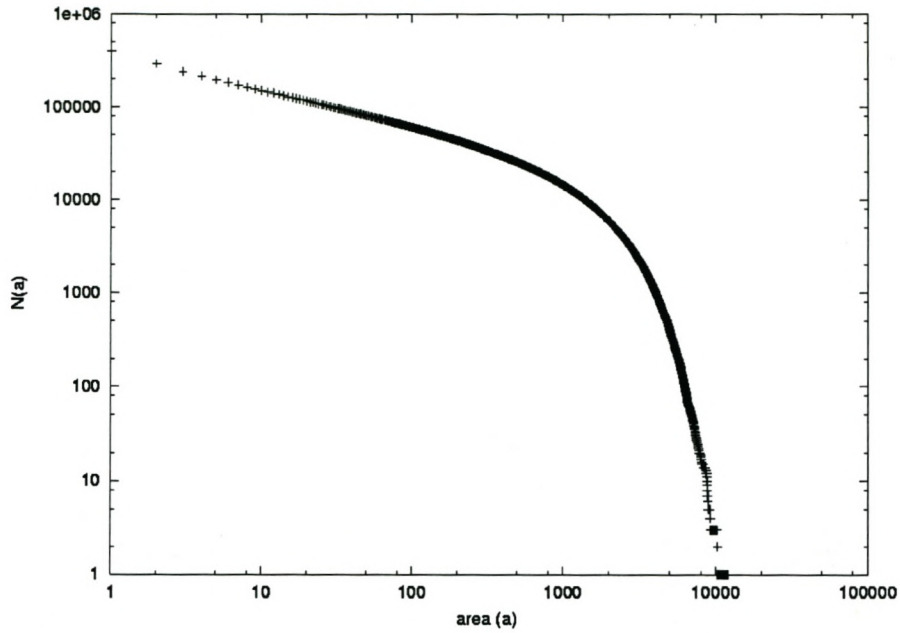

Figure 4.8: The cumulative probability distribution with $p = 1.0$.

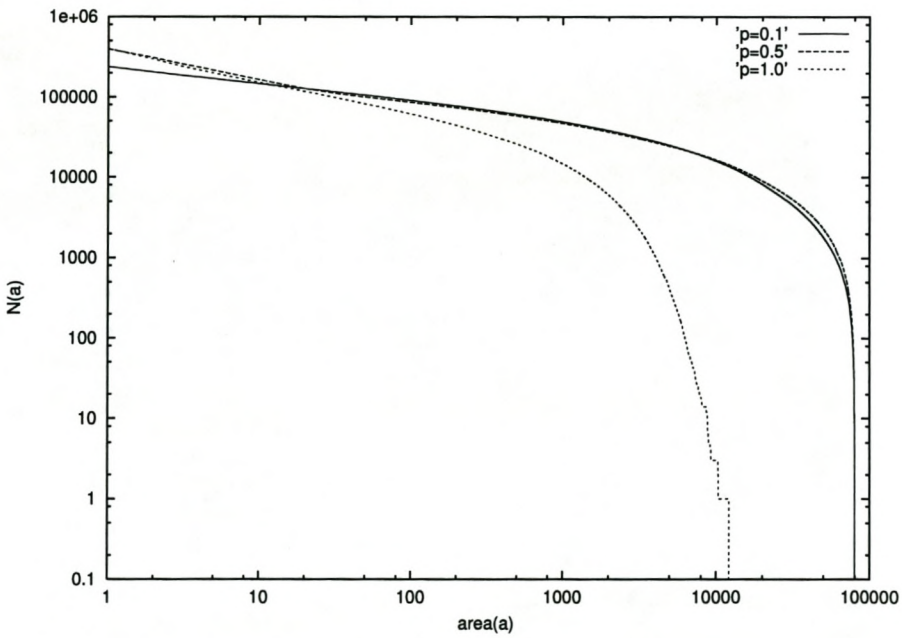

Figure 4.9: The cumulative distributions on a single graph.

4.7 Motivation for the SOC approach to induced seismicity

Apart from the ingredients that helped to define SOC, such as power-law event size probability distributions, threshold dynamics, slow driving, what are the observable consequences of systems that are described by the SOC formalism? In other words, what can one predict and measure about those systems using the SOC framework, other than those things used to define it? In this section we will look at such properties of SOC systems, and then relate them to observations from induced seismicity.

In Chapter 3 we recalled Dhar's detailed analysis of the critical state of the sandpile model using his generalised matrix formulation of the model. As we showed, one is able to compute certain correlation functions, notably the two-point correlation function and the height-height correlation, both of which were seen to be power-laws and thus indicating long-ranged correlations. Within Dhar's formulation it is also possible to compute the fraction of lattice sites that have height $z = 1, z = 2$, etc. We saw that the average height of sand per lattice site reaches an average value about which it then fluctuates. From the analysis of the relative fraction of lattice sites in a particular "state", we see that a reasonable proportion of the lattice is close to the failure threshold whilst the rest of the lattice is fairly robust against perturbations. Sornette and Virieux [40] came to similar conclusions about the strain field, which is proportional to the stress field, of the lithosphere[3] using a non-linear Langevin equation. Their analysis was based on work by Hwa and Kardar [41, 42], who used the same Langevin equation to construct a continuum formulation of the sandpile model of SOC.

In terms of tectonic and earthquake physics and studies of induced seismicity, what does this imply? In other words what are the observable consequences for the earth's crust? Firstly, following from the computation of correlation functions, it implies that the stress field in the earth's crust is long-range correlated. There is not direct evidence that the stress field of the crust is in fact long-range correlated. However, some authors believe that increased seismic activity prior to large earthquakes is a signature of long-range correlations in the stress field. We shall return to this in more detail in the following chapter. Secondly, following from the relative fraction of lattice sites calculation, there are two consequences. One is that a significant portion of the crust is close to failure and a relatively small perturbation can induce seismic activity. This is in fact observed in many cases of induced seismicity (eg. reservoir filling as we pointed out in section 4.3). The second consequence is that due to the fluctuations, not all perturbations of the crust induce seismicity. This is also seen in case studies of induced seismicity [34].

[3]The lithosphere is the outermost 100km of the crust which is relatively rigid and lies on top of the asthenosphere, which is a softer layer of about 400km but which is at a much higher temperature and therefore moves more easily [37].

In hindsight, the conclusions drawn from the calculation of relative occupation of lattice sites seems almost obvious. However, there has been much confusion in the earthquake physics and seismology literature concerning the use of SOC as a modelling framework for seismicity in general. One often encounters the statement that because the system is in a SOC state, the entire crust is close to the failure threshold and that any small perturbation can induce seismic activity. However, as we see from the exposition above, this is clearly not correct.

CHAPTER 5
Frequency size statistics and temporal patterns

5.1 Introduction

In the previous chapters we considered the global statistical properties of the sandpile model. In particular in Chapter 2 we considered the event size probability distribution and in Chapter 3 we reviewed the calculation of correlation functions in the critical state. In the present chapter we look to further establish the correspondence between seismicity and self-organised criticality by considering aspects of the short term temporal behaviour of both types of systems. In particular we consider whether large events can be predicted in some way. The strategy for such an analysis is based on recent ideas that the occurence of large earthquakes is similar to critical points of continuous phase transitions. We further consider under which conditions this assumption holds.

5.2 Dynamic regimes in tectonic seismicity

In this section we briefly discuss a model of fault systems and the evolution of earthquakes, studied by Ben-Zion, Lyakhovsky and co-workers [43, 44], that exhibits both Gutenberg-Richter and characteristic event size statistics. The model to be discussed is designed for the study of the creation and evolution of faults and fault systems.

The model consists of a seismogenic upper crust that overlays a viscoelastic substrate. The upper crust is subject to damage rheology that is compatible with observed nonlinear and irreversible strain. This simply means that the evolving damage modifies the effective material properties of the material in the upper crust. The upper crust is coupled viscoelastically to the substrate, where steady plate motion drives the deformation in the upper crust. The plate motion thus serves as the slow driving for the system.

The model parameters such as boundary conditions, rheological and damage parameters were determined by fitting model calculations to average observed geodetic deformation of the San Andreas fault in California. The remaining parameter of interest, and ultimately the one that controls the dynamic response of the model, is the ratio of the time scale for healing, τ_H, to the time scale for loading, τ_L, i.e., $\frac{\tau_H}{\tau_L}$. The value for τ_H depends on the damage rate coefficient and controls the time for strength recovery after a brittle failure event occurred. The value for τ_L is the time needed for stress to reaccumulate to its threshold value (breaking strength) after a location has failed. This depends on the driving conditions that serve as the external perturbations to the system [43, 44].

The simulation results of Ben-Zion and co-workers [43, 44] show the following. Relatively high values of $\frac{\tau_H}{\tau_L}$ lead to the formation of geometrically smooth or regular fault zones and frequency size statistics consistent with a characteristic earthquake distribution. Characteristic events are the largest possible events on a fault system and are determined by the size of the fault. The term "characteristic" in this context means that the event size is set by characteristics of the fault itself. Low values of $\frac{\tau_H}{\tau_L}$ lead to the formation of highly irregular or geometrically disordered fault zones and frequency size statistics compatible with the Gutenberg-Richter relation. This result is easy to understand in physical terms. Smooth surfaces slide more easily than rough, disordered ones. The highly irregular surfaces will have a more jerky slip associated with them. It is well known in the earthquake physics literature that the earthquake size is proportional to the amount of slip on the fault surface [35]. Intermediate values of $\frac{\tau_H}{\tau_L}$ lead to a seismic response that alternates between these two modes. This is the so-called mode-switching behaviour. In this type of response there are periods of intense seismic activity containing large events and periods of lower intensity where only small and intermediate events are observed.

5.3 Dynamic regimes in sandpile models

The results of the analysis by Ben-Zion and Lyakhovsky motivated us to ask whether there are different dynamical responses for the sandpile model under different conditions. We found that it is possible to access different dynamical response regimes of the sandpile model. To this end we introduce a driving rate for the sandpile model. The driving rate is simply defined as the number of particles added to the system at each time step and is denoted by n. Most of the studies of the sandpile model have focussed on the limit $n = 1$. We now extend the analysis to higher values of n.

The basic model is the same as the BTW model. As already mentioned we now add n particles (where $n \geq 1$) at each time step. This is accomplished in the following way. At each time step n random positions for particle addition are generated. Each of these sites then receive a single particle. These sites are checked for stability and if necessary, they are updated in exactly the same way as the original BTW model. That is, each site that topples discards one particle to each of its nearest neighbours. The order in which the addition sites are updated is irrelevant because of the Aelian property of the model. Recall from the discussion is section 3.3 on the Abelian property that the order in which unstable sites are toppled is irrelevant for the final configuration. Also recall from section 3.3 that the operations of adding a particle and toppling unstable sites commute. Thus, the same final lattice configuration will be reached whether you add n particles simultaneously to randomly selected sites or whether you add them sequentially

to the same set of sites and allow the system to relax at each time step.

The question may well be asked why we are interested in adding the particles simultaneously if the same final configuration will be reached if you add them sequentially. The important point under consideration is not the final configuration that is reached, but rather the system response to a particular perturbation. Admittedly the nett input into the system is the same whether we set (say) $n = 10$ or whether we wait for 10 consective time steps, picking the same set of sites. As we shall see, the response of the system is very different for the two situations. The Abelian property in this case merely provides a very convenient computational simplification.

We now show the analogous roles played by the driving rate in the sandpile model and the ratio $\frac{\tau_H}{\tau_L}$ in the Ben-Zion - Lyakhovsky model. Large n corresponds to large values of $\frac{\tau_H}{\tau_L}$ and vice versa. This can be motivated as follows. In the sandpile model there is no real equivalent of τ_H so we arbitrarily set it equal to a constant, say 1. The definition for the loading time is exactly the same as in the tectonic context, i.e., the time for reaccumulation of stress to its threshold value at a failed site. Consider the special case of loading a fixed site. This leads to no loss of generality since it is quite possible to select the same site at four consecutive time steps. Suppose our loading site topples during an avalanche and let us assume it is the only site to topple (avalanche of size $a = 1$). If the driving rate is $n = 1$, it will take 4 time steps for the site to reach its maximum value again, and therefore $\tau_L = 4$ and $\frac{\tau_H}{\tau_L} = \frac{1}{4}$. If, on the other hand, the loading rate is $n = 4$, say, it will take 1 time step to reach the maximum value, and thus $\tau_L = 1$ and $\frac{\tau_H}{\tau_L} = 1$. The correspondence between n and $\frac{\tau_H}{\tau_L}$ then follows.

From simulations we have the following results. For small values of n the sandpile model response is that compatible with power-law Gutenberg-Richter type frequency size statistics and for large values of n that of a characteristic event size distribution (see Figures 5.1 and 5.2 for the event size distribution). Thus, there are also at least two dynamical response regimes for the sandpile model that is controlled by the driving rate.

5.4 Time-to-failure concept

In recent years it has been proposed that the occurence of large earthquakes can be compared to critical points of continuous phase transitions. In this section we will discuss this concept in some detail as well as the conditions under which the analogy is valid. Before we do this, for the sake of completeness, we briefly repeat parts of the discussion presented in chapter 1 on the basic results of continuous phase transitions.

The critical point is characterised by the existence of long-range correlations between the basic degrees of freedom of the system under consideration. More specifically, close to the critical point

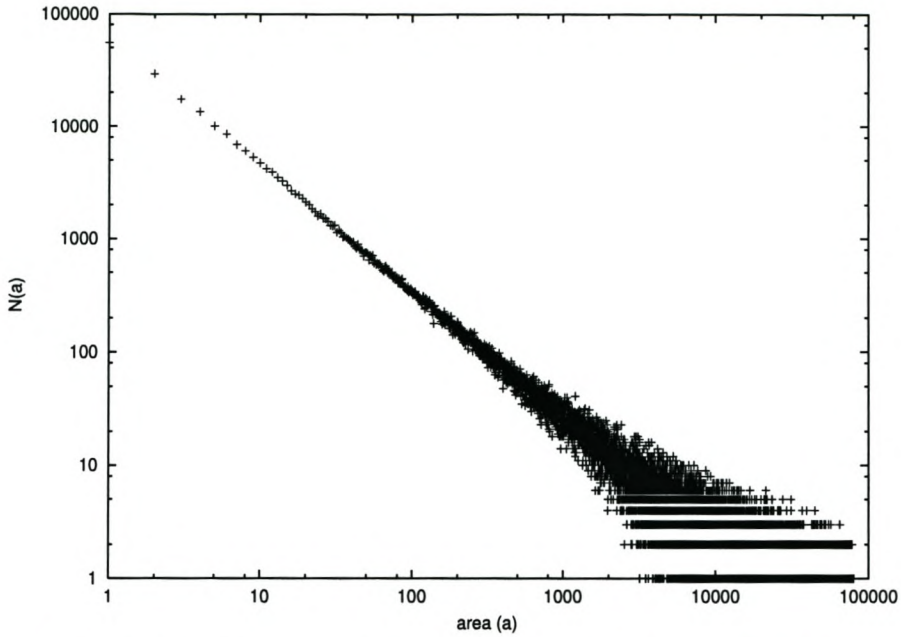

Figure 5.1: The non-cumulative event size distribution for the BTW sandpile model for driving rate $n = 1$.

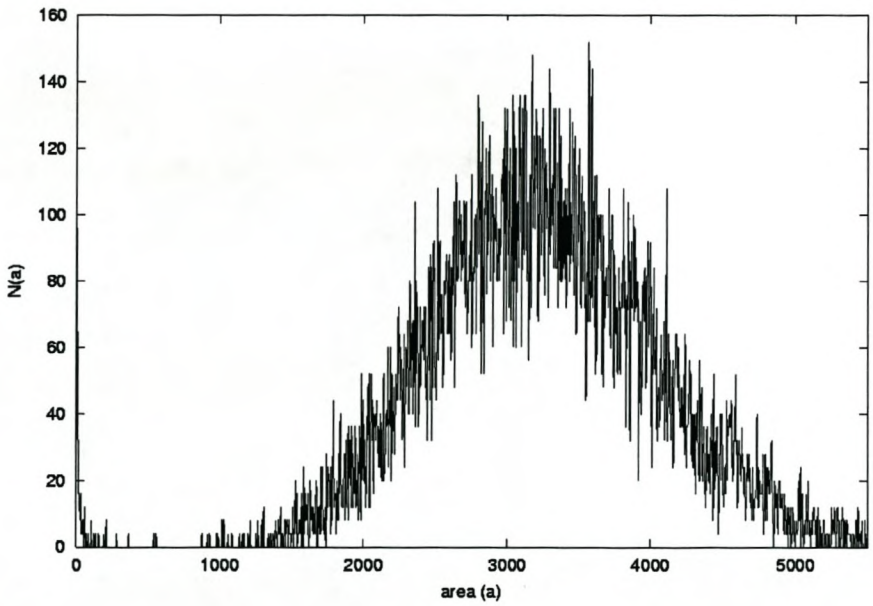

Figure 5.2: The non-cumulative event size distribution for the BTW sandpile model for driving rate $n = 40$.

the correlation length is given by the relation

$$\xi \sim |T - T_c|^{-\nu}. \tag{5.1}$$

We see that the correlation length grows as a power-law as the critical point is approached and eventually diverges at the critical point. It is not only the correlation length that displays this power-law form in the region of the critical point, but also all other measurable observables. For example, the magnetisation of the Ising model is given by the expression

$$M \sim |T - T_c|^{\beta}, \tag{5.2}$$

which is a further reflection of the scale invariance at or close to the critical point as implied by (5.1).

It was said above that the occurence of large earthquakes is believed to be analogous to critical points of continuous phase transitions. This is motivated by the fact that many large earthquakes are preceded by an increase in seismic activity prior to the large event. Specifically, the number of intermediate to large earthquakes increase as the time of the large event is approached. It has been found that the increase in activity prior to large earthquakes is described by the following relation;

$$A(t) = B + C(t_c - t)^{\alpha}, \tag{5.3}$$

where $A(t)$ is the cumulative seismic activity at time t and t_c is the time of occurence of the large event and B and C are constants determined by fitting the data. The exponent α is found to have values between 0 and 1 and $C < 0$.

This still did not explain why the cumulative seismic activity increases as the time of occurence of the large event is approached. In 1995 Sornette and Sammis [45] proposed that large earthquakes are similar to critical points of continuous phase transitions and that they occur due to progressive correlations in the stress field that build up in a region surrounding the location of the large event. These progressive correlations in turn lead to events at increasing length scales which is reflected in the increasing number of intermediate to large events as the large event is approached. The relation to continuous phase transitions is thus embodied in the power-law increase in cumulative seismic activity as one approaches t_c. In terms of the analogy, t_c now plays the role of the critical temperature, T_c and the cumulative seismic activity, $A(t)$ in this case, that of the observable quantities that scale as power-laws in the approach to the critical point.

Apart form its obvious theoretical value, the above formalism also provides a framework for predicting large earthquakes. This is achieved by fitting the cumulative seismic release to the relation (5.3) in which B, C and α are parameters of the fit. In section 5.5 we will discuss the basic algorithm used to predict large events.

An important question is of course under which conditions one will observe such critical behaviour prior to large earthquakes. If a system is in a stationary state, the contribution of each event to the cumulative activity is exactly the same as that of its predecessor [46]. That is, A_i is the same for all i or stated differently, the activity rate is time-independent. By activity rate we simply mean the average event size per unit time. Plotting the cumulative activity for a stationary state as a function of time one obtains a straight line. That is, if $A(t)$ is the cumulative value of the parameter of interest at time t, then

$$A(t) = Bt + C, \tag{5.4}$$

where B and C are constants.

The gradient of this line is the activity per unit time. This type of response could be termed a "typical" response of the system to an external perturbation since under the same driving conditions the system always gives this response. The event size probability distribution will in this case be peaked about the value corresponding to the typical response. We have seen that for the sandpile model and the model of Ben-Zion and Lyakhovsky for tectonic earthquakes this type of probability distribution corresponds to large values of n and $\frac{\tau_H}{\tau_L}$ respectively.

It still remains to see what happens if the system is not in a stationary state. It has been proposed that the evolution of the system takes place in terms of episodes from one critical event to the next and that event sizes in the period between critical events are distributed according to a power-law like the Gutenberg-Richter [46].

In summary thus, the basic idea is that if the events follow a power-law distribution in their size, they will exhibit power-law time-to-failure behaviour as given by eq. (5.3). If they follow the characterisitic event size distribution there will be no signs of power-law acceleration prior to large earthquakes and the cumulative seismic activity simply increases linearly in time according to (5.4). As mentioned above we will discuss the algorithm for performing time-to-failure analysis in the following section. In section 5.6 we discuss the results of the time-to-failure analysis for the Ben-Zion - Lyakhovsky model of tectonic seismicity (see section 5.2) and the relation to the probability distribution function of the events. Thereafter we discuss the results of a time-to-failure analysis for real mining-induced seismicity data and and in section 5.8 we present the results for the same analysis for the BTW sandpile model.

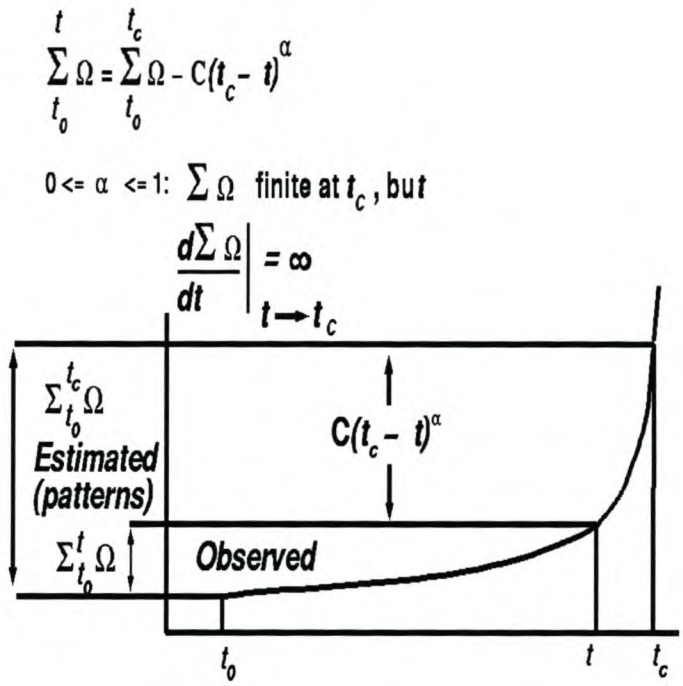

Figure 5.3: Graphical representation of critical accelerating behaviour by a variable (power-law behaviour). Reproduced from [46]

5.5 Time-to-failure algorithm

As was explained in the previous section the critical event hypothesis was first introduced in the context of tectonic earthquake phenomena. We also said there that it provides one with a framework for predicting large earthquakes. In this section we give a description of the algorithm used to perform forward prediction of large events. The procedure we will outline here was developed for the analysis of mining-induced seismic data but also used in establishing the critical event concept in the sandpile model data.

The tools for performing the analysis were developed by Willem de Beer (formerly of ISS International) as part of a research contract for the Safety in Mines Research Advisory Committee (SIMRAC) [46]. The practical output of the research was a working program that tests the critical event hypothesis in the mining-induced seismicity context and at the same time has the functionality to predict such critical events using the hypothesis. Without discussing the technical details we will briefly outline the basic algorithm used.

As already mentioned in section 5.4, the prediction strategy is based on the hypothesis that large seismic events are similar to critical points of continuous phase transitions. We saw that in the seismic context this translates to large events being preceded by an acceleration in the seismic activity. Specifically the accelerated increase follows a power-law in the time to the large

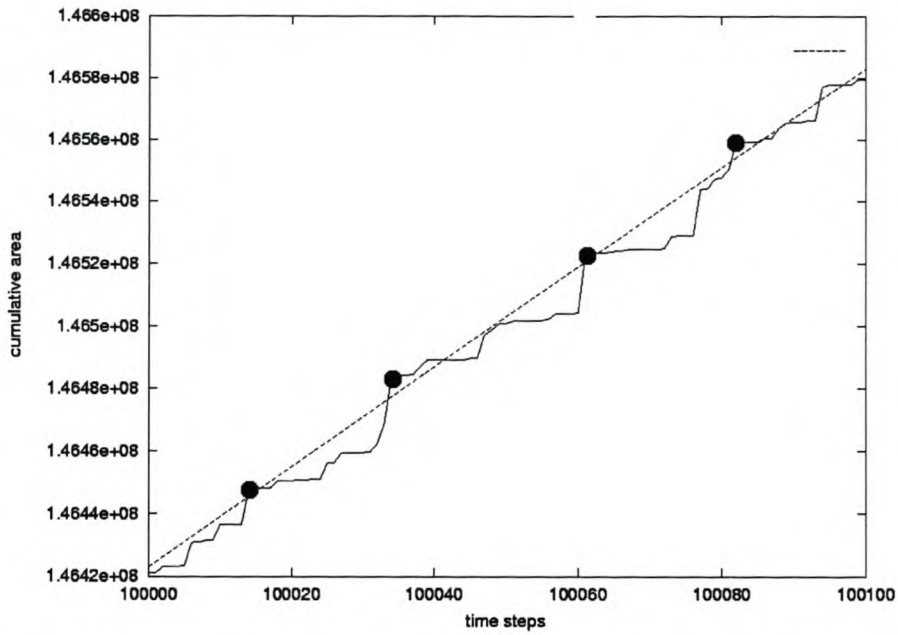

Figure 5.4: Schematic illustration of the linear relation between episodes of cumulative activity using sandpile model data. The critical events are indicated by the solid circles.

event. Mathematically this is given by the relation

$$A(t) = B + C(t_c - t)^{\alpha}. \tag{5.5}$$

This equation simply says that the cumulative activity follows a power-law in the time to the large event at t_c.

For real prediction purposes one is interested in knowing when a large seismic event will take place and what its magnitude will be. In terms of the critical event formalism this means one would like to obtain the parameters A_c, t_c, C and α in (5.5) from fitting the data at time t. Here we have denoted the critical event size by A_c. The left hand side of eq. (5.5) contains the observed seismic parameters at time t (see Figure 5.4).

In order to ensure that the inversion routine used to obtain the above mentioned parameters does not get trapped in a local minimum a positive feedback loop was developed in which the algorithm learns the characteristics of the system. There are three phases for the algorithm in the prediction process. The first phase, where the algorithm learns about the characteristics of the system, is called the "learning phase". The other two phases are known as the "learning to predict" and "the prediction" phases respectively.

5.5.1 The Learning Phase

The steps in this phase are summarised by the following main points:

- There exists an empirical relationship between the constant C in (5.5) and the size of the critical event A_c [46]. The relation is

$$\log C = K + P \log A_c. \tag{5.6}$$

  An initial set of large events is used to establish this relationship. This serves to eliminate one parameter from the inversion routine.

- Episodes of cumulative activity that culminate in critical events, are related by a simple linear relation in time (see Figure 5.4). This linear relationship is established.

- The periods between large or characteristic events are searched for power-law sequences which exclude the characteristic events. The average and median of $t_c - t_{c-1}$, as well as relevant standard deviations are calculated. t_{c-1} denotes the time of occurrence of the last event before the critical event.

- Average and median critical exponents, α and higher moments are established.

- The average and median of the critical event size, A_c, and higher moments are computed.

5.5.2 Learning to Predict Phase

Once the learning phase is complete and the algorithm has learnt the characteristics of the system, it can now learn how to predict. For this phase a further set of critical events is used. The procedure for this phase is summarised as follows:

- The constant C in (5.5) is replaced by the relation (5.6) which relates the size of the critical event and C.

- A first estimate for the cumulative activity at t_c is made by extrapolating the linear relation between the episodes of critical events (the relation illustrated in Fig. 5.4).

- The moments of the exponents and $t_c - t_{c-1}$ are used as the first estimates for the inversion.

- Starting from six events after a critical event, the inversion is performed if an event is the termination of a power-law sequence.

- A prediction is issued if the predicted size of the critical event, A_c and time of failure, t_c, falls within two standard deviations from the means computed in the learning phase.

- The average and median errors and higher moments of the predicted quantities are computed.

This concludes the learning to predict phase.

5.5.3 The Prediction Phase

The algorithm continues in the same way as in the previous two phases. However, the inversion is now perturbed by the errors in the prediction as calculated before. Alerts are issued when the predicted values for the size of the critical event and t_c fall within two standard deviations from the mean values calculated in the learning phase.

5.5.4 Computation Time

We thus see that the process of predicting large events as discussed above is quite complex. It requires considerable computing power and sufficient data to establish the patterns in a given area. As already mentioned above, the same procedure was used in the sandpile model analysis. Even for the simple sandpile model the computations described above require considerable computing time. For example, for a lattice of linear size $L = 100$, considering 21 different simulations with driving rates $n = 1, 2, 4, 6, \ldots, 40$ respectively and each containing about 5×10^5 avalanches, it took more than two weeks just to establish the learning phase of the model.

5.6 Time-to-failure for fault systems

Ben-Zion and Lyakhovsky [44] analysed the temporal statistics of the model discussed in section 5.2 by considering the cumulative Benioff strain as a function of time (see Figure 5.6). The Benioff strain is defined as $\sqrt{M}$, where M is the seismic moment, defined in Chapter 4.

Part A of Figure 5.6 is the cumulative Benioff strain for seismicity having the characteristic event size distribution. It is clear that the cumulative activity is approximately linear, with no episodic behaviour. In part C of Figure 5.6 we have the cumulative Benioff strain for seismicity corresponding to a Gutenberg-Richter distribution. There is clear evidence of accelerated seismic activity prior to a large event. According to the analysis of Ben-Zion and Lyakhovsky [44] the accelerated increase follows a power-law in the time-to-failure. For the case of mode-switching behaviour (part B of Figure 5.6) the first period is a straight line, associated with a characteristic event size distribution, whereas for the second period associated with Gutenberg-Richter statistics, there is a weak accelerating phase before the large event in that period.

The simulation results of Ben-Zion and Lyakhovsky [44] seem to be consistent with (1) the suggestion that the cumulative activity is stationary when the individual events are distributed

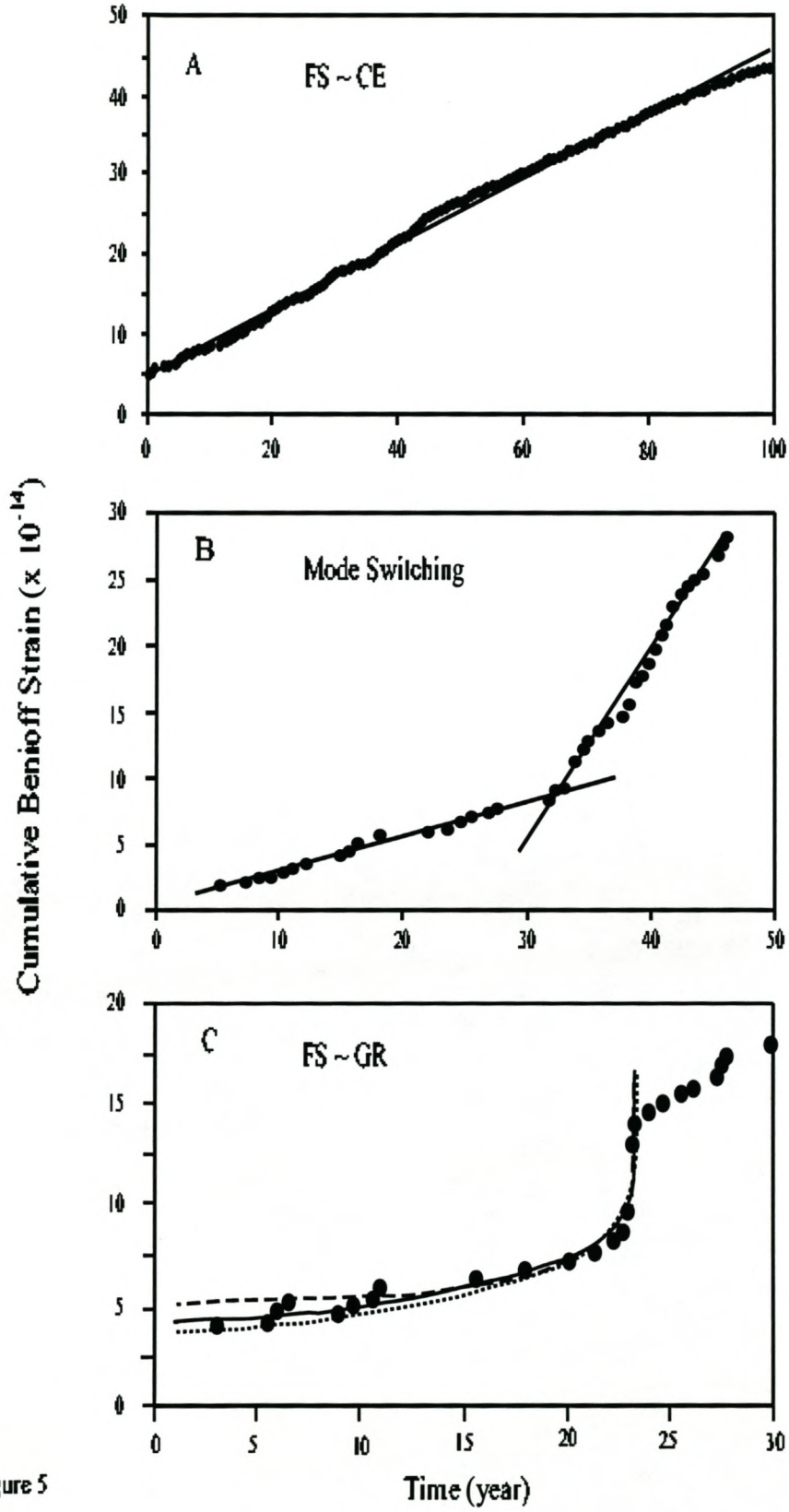

Figure 5.5: Cumulative Benioff strain from damage rheology model. Reproduced from [44]

according to a characteristic event size distribution and, (2) there is power-law accelerated activity prior to large events if the individual events follow the Gutenberg-Richter law.

5.7 Time-to-failure in mining-induced seismicity

We now turn our attention to the situation in mining-induced seismicity. In particular, we consider the work of de Beer [46] that focusses on establishing whether accelerated seismic release is observed prior to large events in mining-induced seismicity as well.

The first important point is the choice of suitable variables for the analysis. During the course of the research conducted in [46] nine different variables were considered, but three were eventually decided on. These are,

1. Cumulative Benioff strain, $\sum\sqrt{M}$
2. Cumulative square root of radiated seismic energy, $\sum\sqrt{E}$
3. Cumulative Apparent volume, $\sum V_A$.

The second important aspect of the analysis is the choice of the volume and time windows in which to search for accelerated activity. Stated differently, one is searching for the region and time window over which the stress field becomes correlated. Before we show how such a region is selected we introduce a few concepts that will be needed in the discussion. When considering real seismic data it is important to be able to estimate which of the linear or power-law fits to the cumulative activity gives a more accurate description of the data. This is done in the following manner [46]. The cumulative seismic quantity of interest, $\sum_{i=n}^{c} A_{t_i}$ is computed, and then fitted to a power-law,

$$S_p(t) = C(t_c - t_n)^{\alpha} \tag{5.7}$$

and a linear equation,

$$S_l(t) = C + Bt, \tag{5.8}$$

where the $S(t)$ denotes the cumulative seismic parameter at time t. The variances

$$V_p = \sum_{k=1}^{c}\left[S_p(t_k) - \sum_{i=0}^{k} A_{t_i}\right]^2 \tag{5.9}$$

and

$$V_l = \sum_{k=1}^{c}\left[S_l(t_k) - \sum_{i=0}^{k} A_{t_i}\right]^2 \tag{5.10}$$

are then computed and compared. The ratio $r = \frac{V_p}{V_l}$ gives an indication of which of the two hypotheses gives a better fit to the data. For large values of r the linear fit is more appropriate, whereas for small r, the power-law in the time-to-failure is more accurate. If $r = 1$, we cannot say which of the two fits gives the best fit to the data.

We now briefly outline the strategy for selecting optimal windows in space and time [46, 47]. The volumes are all taken as circular or spherical around the location of the critical events in [46]. For a given event, a minimum radius is fixed and time windows of $24, 48, 72, 96, \ldots$ hours are considered and the ratio r, defined above, calculated. The time window for which r is minimal, as well as the corresponding value of r are stored. The volume radius is then increased by 100m and the process repeated until the spatial limit of the data catalogue is reached. Finally, the minimum r value for each spatial window is plotted as a function of the radius of the circular area. The parts of the curve where r is minimal help to define a suitable radius within which to search for power-law behavior preceding the large event of interest.

In section 5.4 we mentioned that the time-to-failure analysis presents a strategy for predicting large earthquakes. However, in the discussion as outlined in section 5.4, it is assumed that one has the time of the large event, t_c, fixed and merely attempts to fit the data to obtain the parameters B, C and α of the equation (5.3). On the other hand, if one is trying to predict the time of the large event t_c has to be obtained as one of the parameters of the fit. We discussed the basic algorithm for performing forward prediction in section 5.5. De Beer discusses the results of such forward prediction of mining-induced seismic data at length in [46] and we will not attempt to do so here.

In the rest of this section we discuss the results of a back-analysis of real mining-induced data which tested for the accelerated activity prior to 9 large events. The purpose is simply to illustrate that such accelerated activity has been observed in mining-induced seismic data.

De Beer considered a data catalogue containing about 30000 events and spanning a time period of one year. In this case the first nine events with $\log_{10} M \geq 12$ are considered as the critical events. The results of the analysis are summarised in Table 5.1.

The table contains a column for the power-law accelerated activity exponent, α, as defined in eq. (5.3) as well as the r ratio for both 2 and 3 dimensional analyses. For each event, a seismic variable with an entry in the exponent column, shows power-law accelerated activity prior to the large event. For example, for event no.2 there was no power-law acceleration prior to it, whereas for event no. 3 there was accelerated seismic activity only in the cumulative apparent volume. The table indicates that eight of the nine events show accelerated release in at least one of the seismicity variables. The table also shows the results for the analysis being performed in

Event	Variable	α		r	
		3D	2D	3D	2D
1	$\sum\sqrt{E}$	0.232	0.232	0.211	0.211
1	$\sum\sqrt{M}$	0.228	0.228	0.234	0.234
1	$\sum V_A$	-	0.189	-	-
2	$\sum\sqrt{E}$	-	-	-	-
2	$\sum\sqrt{M}$	-	-	-	-
2	$\sum V_A$	-	-	-	-
3	$\sum\sqrt{E}$	-	-	-	-
3	$\sum\sqrt{M}$	-	-	-	-
3	$\sum V_A$	5.040	5.040	0.468	0.468
4	$\sum\sqrt{E}$	-	0.627	-	0.230
4	$\sum\sqrt{M}$	-	0.521	-	0.199
4	$\sum V_A$	-	-	-	-
5	$\sum\sqrt{E}$	-	0.570	-	0.000
5	$\sum\sqrt{M}$	-	0.054	-	0.000
5	$\sum V_A$	-	-	-	-
6	$\sum\sqrt{E}$	0.585	0.670	0.081	0.107
6	$\sum\sqrt{M}$	0.612	0.928	0.141	0.202
6	$\sum V_A$	-	0.472	-	0.429
7	$\sum\sqrt{E}$	0.286	0.286	0.047	0.047
7	$\sum\sqrt{M}$	0.364	0.365	0.048	0.049
7	$\sum V_A$	-	0.731	-	0.117
8	$\sum\sqrt{E}$	0.087	0.118	0.251	0.117
8	$\sum\sqrt{M}$	0.054	0.327	0.297	0.000
8	$\sum V_A$	-	-	-	-
9	$\sum\sqrt{E}$	-	-	-	-
9	$\sum\sqrt{M}$	-	-	-	-
9	$\sum V_A$	-	1.540	-	0.000

Table 5.1: Summary of the time to failure analysis of mining-induced seismicity data

$2D$ and $3D$. In the $3D$ case the actual vertical location of the events were taken into account, whereas in the $2D$ case all events were considered to be in the plane of the ore body. The reason for this is that in general the vertical location of the seismic events is problematic. We see that in some cases (events 4, 5 and 9) neglecting the vertical location indicated accelerated release whereas including it did not. Also, for those cases where both the $2D$ and $3D$ analyses indicate accelerated release, the difference in value of the exponent α is not large.

5.8 Time-to-failure in the BTW sandpile model

In this section we discuss the results of a time-to-failure analysis performed on BTW sandpile model data. As mentioned earlier, this is done because of our belief that the sandpile model

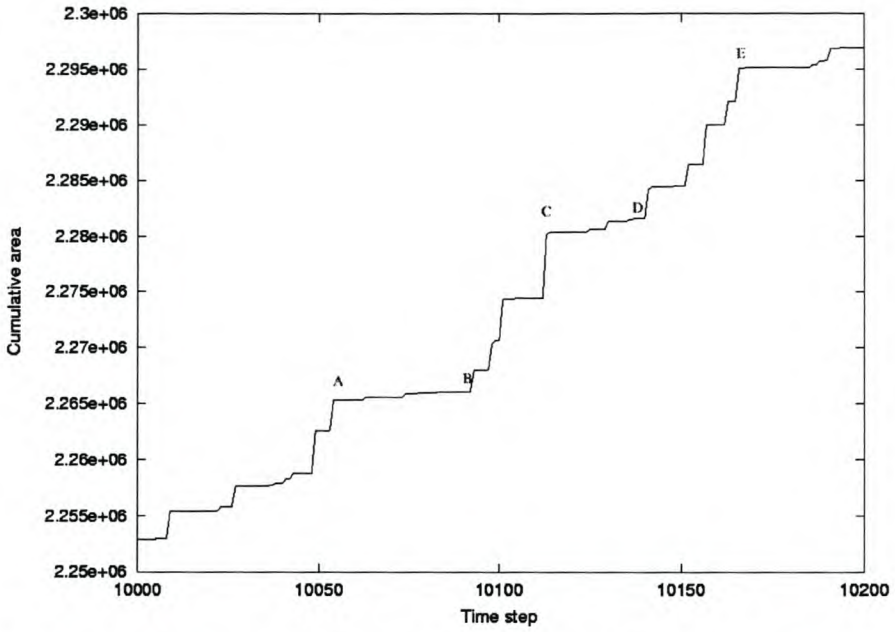

Figure 5.6: The cumulative area for the sandpile model as a function of time for driving rate $n = 1$ for a lattice of linear size $L = 100$.

represents a simple model that captures the essential features of seismicity. One thus expects similar behaviour for the sandpile model evolution as observed in the case of seismic data. We also explicitly consider the conditions under which the time-to-failure analysis is valid in this model by considering the percentage of critical events that are preceded by power-law acceleration of activity as a function of the driving rate of the model. As we saw in section 5.3, different driving rates lead to different response regimes as encoded by the event size probability distribution functions.

For the sandpile model, we chose the area affected by avalanches as our measurable quantity with which to perform the analysis. In all the simulations we used $a = 0.59N$ as the critical event size, where N is the number of lattice sites. The motivation for this particular choice is given in the following section. The cumulative area affected by avalanches (simulated on a 100×100 lattice), is plotted for a time window of 200 time steps in Figures 5.6 and 5.7 for driving rates $n = 1$ and $n = 40$ respectively. For the slow driving limit there is clear evidence of episodic behaviour. After large events there are periods of relatively little activity (A to B and C to D in Figure 5.6) which are followed by periods of accelerated activity (B to C and D to E in Figure 5.6) prior to the next large event. The average value for the exponent α for this driving rate is 0.351. This is within the range $0 < \alpha < 1$ which is generally found from fits of tectonic and induced seismicity data. For the fast driving limit the activity rate is more or less stationary

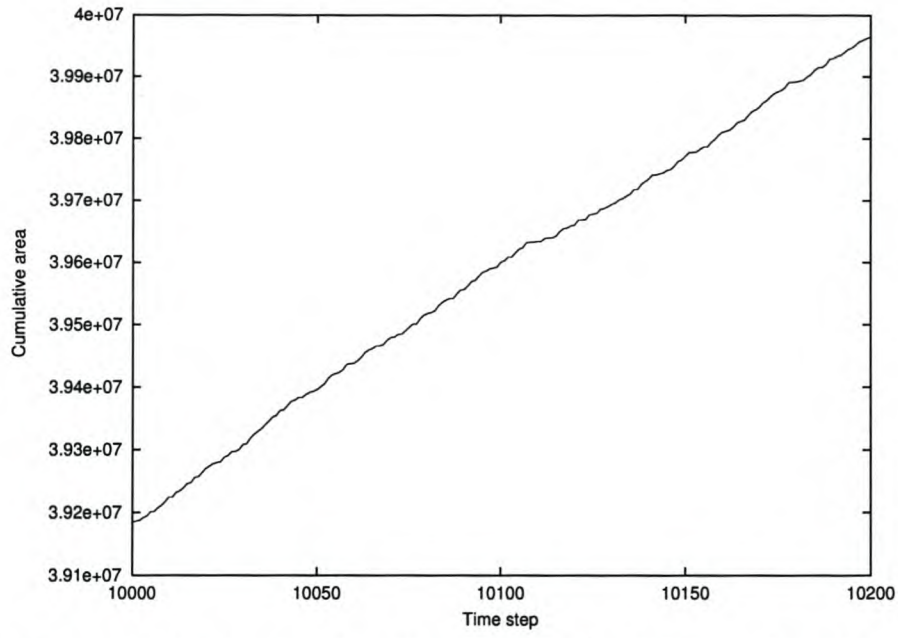

Figure 5.7: The cumulative area for the sandpile model as a function of time for driving rate $n = 40$ for a lattice of linear size $L = 100$.

with no discernible episodes as seen from the almost straight line for the cumulative activity with time. This observed straight line is in agreement with the form suggested by eq. (5.4).

In Figure 5.8 we plot the percentage of critical events preceded by power-law acceleration of activity in the time-to-failure as a function of the driving rate. For the case of $n = 1$, 81.31 percent of critical events were preceded by power-law time-to-failure increase in activity, whereas for $n = 40$ only 0.30 percent of critical events were preceded by such power-law acceleration. We thus see that this is highest for small driving rates, further confirming the assertion that phases with power-law event size distributions show power-law increase in activity prior to large events.

In section 5.5 we discussed the basic algorithm used to make forward predictions of large events. We did not consider the case of forward prediction in the sandpile model due to limited available computing time. As pointed out in section 5.5, performing such analyses is computionally intensive and we thus decided to limit our investigation to establishing whether accelerating activity is observed prior to large events in the sandpile model and if so, the conditions under which it will be observed.

Let us briefly comment on the behaviour of the system in the different response phases. First consider the Gutenberg-Richter phase. In a complex, disordered material, the stress is not uniformly distributed or perturbed by the external driving force. Initially small regions of excess stress are created and the energy released from these clusters is small. The release from

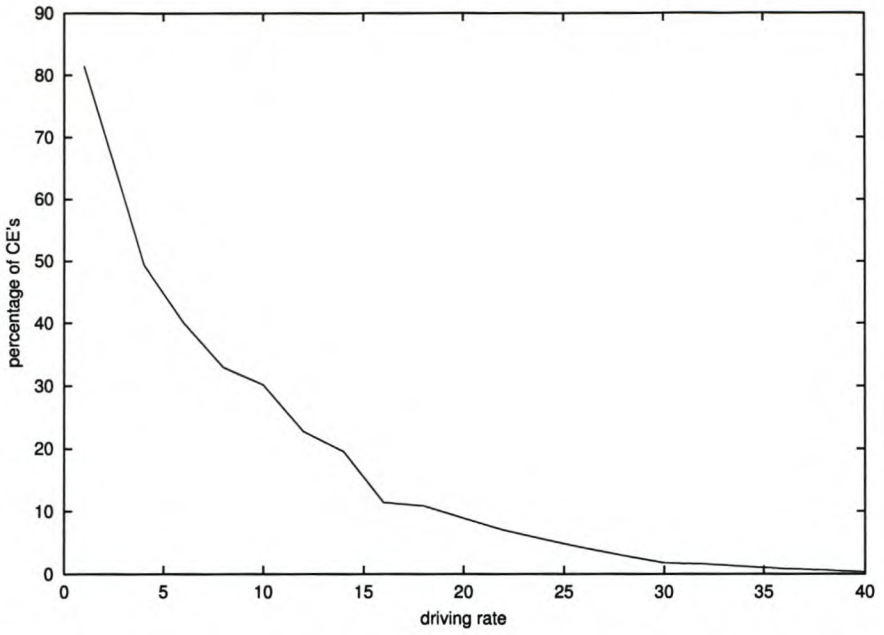

Figure 5.8: The percentage of characteristic events preceded by power-law acceleration in the release as a function of driving rate for a lattice of linear size $L = 100$.

these clusters is also not uniform, and this gives rise to the scaling (power-law) regime of the Gutenberg-Richter relation. This can be viewed as a self-organising phase during which, if the driving force is slow enough, stress is progressively transferred to larger and larger clusters that are close to failure.

In the phase with characteristic event size statistics, stress is not distributed to larger clusters progressively. It can be imagined that the system remains in a state where large clusters of sites that are close to failure are always present. It is as if the system remains in a state with long-range correlations.

5.9 Critical events

In this section we briefly discuss the critical event concept and its origins in more detail. We also motivate our choice of critical event size in the sandpile model.

The concept of a critical event has its origin in trying to understand the mechanism by which disordered materials rupture [37, 48]. There are several strategies to modelling this rupture process. The most basic models assume that crack growth is similar to a percolation transition in that when a macroscopic crack spans the material, global breakdown has occured. Several models that go beyond just a simple percolation type analysis have been developed over the years [37]. These models try to incorporate the dynamical aspects such as stress redistribution

[37]. All of these models point to the fact that large scale breakdown occurs at some critical value of stress or density of micro-cracks. The basic physical picture is that one starts off with isolated randomly located defects or micro-cracks that grow under the increased loading stress or with time until a "critical" density of defects or micro-cracks per unit volume is reached. This then signals global breakdown of the material under consideration. Most of the models show an acceleration of cumulative damage or cumulative energy released as these critical density or stress values are approached. This accelerating behaviour is found to be described by

$$D \sim A + B(\sigma_c - \sigma)^z, \tag{5.11}$$

where D is some measure of the cumulative damage in the sample and σ is the stress applied to the material and σ_c is the stress at which breakdown occurs. This is exactly of the same form as eq. (5.3).

Such critical point behaviour has also been observed when testing the breakdown of real materials. In refs. [37, 48] Sornette describes tests performed by the French Aerospace company Aerospatiale on real composite materials that are used in the manufacturing of pressure tanks. Tests of the breakdown properties of these tanks reveal such critical point behaviour as described by eq. (5.11).

These studies and experiments form the basis on which the critical event concept for tectonic earthquakes was introduced. It is also interesting to note that in the early 1980s there were already suggestions that large earthquakes correspond to some critical breakdown phenomenon. This was made on the basis of a renormalisation group study of a model that simulates the mechanical breakdown of materials [49]. In conclusion, the critical event concept is based on the fact that large scale breakdown occurs at a specific value of some parameter of the system under consideration and it is preceded by a power-law increase in the cumulative activity.

We now turn to the question of our particular choice of $a_c = 0.59N$ for the critical event size in the sandpile model simulations. The most convenient way to think of how to choose the critical event size is to make a connection with percolation theory. This approach is motivated by studies of the Forest Fire Model by Turcotte and co-workers [50]. We first give a description of the Forest Fire Model in two dimensions. Consider a lattice where each site can be either occupied by a tree or empty. At each time step a random site is selected and if the site is empty a tree is planted there. If the site is occupied, a new random site is selected. Trees can also be removed from the lattice by so-called fires that are ignited with a sparking frequency f. This means that every $\frac{1}{f}$ time steps, instead of planting a tree, a spark is dropped om a randomly selected site. If a site is occupied by a tree, it burns and all nearest neighbour sites that are

occupied also burn. If a site is empty when a spark is dropped, nothing happens and the planting process continues at the next time step. One can think of the dynamics of the forest fire model as a competition between growing and destryoing clusters of trees. The Forest Fire Model has also been shown to exhibit SOC behaviour in that the distribution of fire sizes (defined as the number of trees burnt in a fire), and the distribution of cluster sizes both display power-law behaviour [2, 50].

We now discuss the relation between the Forest Fire Model and site percolation as studied by Turcotte and co-workers [50]. Site percolation is defined on a lattice where each site can either be occupied or empty. At each time step a site is randomly selected and if it is empty it receives a particle. If the site is already occupied nothing happens and the next random position is generated. It is well known that in 2 dimensions the critical density where a connected cluster of occupied sites spans the lattice is $\rho_c = 0.59275$ [50]. Here the density is defined as $\rho = \frac{p}{N}$ where p is the number of occupied sites and N is the total number of lattice sites. It is clear that the forest fire model without any fires is exactly a site percolation problem. It is precisely this forest fire model without fires that Turcotte et al. considered in making the connection between site percolation and the forest fire model [50]. Thus, a Forest Fire Model without fires will have a connected cluster of trees that span the lattice when the density of trees is 0.59275 of the total number of lattice sites. Consider dropping sparks on the lattice again. If one were now to drop a spark and hit a tree, the ensuing fire would span the lattice with size $a_F = 0.59275N$ where we denote the area covered by the fire by a_F.

Now consider the sandpile model. Just as the fires were "switched off" in the forest fire model, consider a sandpile model where one temporarily does not allow avalanches to occur. Every site is still limited to have a maximum of 4 particles, but if a site reaches its threshold it is not allowed to topple. Continuing in this way one will reach a stage where sites with height $z = 4$ (those that can topple when they receive a particle) will form a connected cluster that spans the lattice. Careful consideration will reveal that this is equivalent to the forest fire model without fires. Sites with $z = 4$ now replace the trees that can burn. A convenient way to think of it is to consider the sites with height $z = 4$ as "occupied" and all other sites as "empty". This is of course equivalent to the site percolation problem and the critical density of sites that will participate in an avalanche when perturbed is the same as the percolation density of site percolation. Thus we choose $a_c = 0.59N$ as the critical event size.

We realise that there are some problems associated with this site percolation approach for the sandpile model. It is much easier to implement it in the forest fire model since there are two distinct "operations" that govern the dynamics of the clusters of trees. Planting trees grow

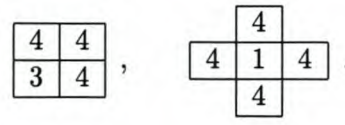

Figure 5.9: Examples of induced topplings during an avalanche

clusters whereas dropping sparks destroy them. By simply taking the sparking frequency small enough one can grow clusters large enough that will allow system spanning fires. In the sandpile model the same operation that adds particles, and hence grows clusters of sites with $z = 4$, is also responsible for inducing avalanches and thus destroying these clusters. One thus cannot control when avalanches will occur and they may be induced before one has system spanning clusters of sites susceptible to toppling. However, one finds that topplings can be induced on sites that do not have their heights equal to 4 when the avalanche is initiated (see Figure 5.9). In first example the site with height $z = 3$ will also topple if any of the sites with height 4 topple during an avalanche. Likewise in the second example the site with height 1 is not included in the cluster of susceptible sites, but it will topple if each of its neighbours topple during an avalanche.

The hope is thus that the effects of (1) not being able to control when avalanches occur and (2) these so-called "induced" topplings more or less cancel each other so that the site percolation density value is still a valid approximation for the critical event size. This of course has to be checked carefully. However, from the results of the sandpile model data of the previous section it would seem as if this choice provides a good first approximation to the critical event size. The percolation argument for the sandpile and forest fire models also makes a connection with the discussion at the beginning of this section on the breakdown of materials where the large scale breakdown is assumed to be some sort of percolation transition.

We now briefly discuss another approach, due to Chakrabarti and co-workers [51, 52], to analyse large events in the BTW sandpile model. The basic question is again whether large events correspond to a critical value of some parameter of the model? In other words, is there some measurable property of the sandpile model that assumes a critical value when large or system spanning events take place? The average height, h_{av}, of the sand columns turns out to be a good indicator of such critical behaviour. Large events occur when h_{av} reaches some critical value, h_c. Again, as was previously discussed for the time-to-failure approach, if this is a critical point, the approach to criticality should be signalled by power-law behaviour of the measurable quantities.

In their analysis Pradhan and Chakrabarti [52] considered how the number of topplings in

an avalanche, s, the relaxation time, τ, and the correlation length behave as the critical point is approached. The first of these two parameters were already defined in Chapter 2 of this dissertation. The correlation length is here defined as the average distance between the addition site and the furthest site that toppled during an avalanche. In their numerical studies Pradhan and Chakrabarti found that all three quantities show power-law divergence as h_c is approached. That is,

$$\tau \sim (h_c - h_{av})^{-\gamma} \tag{5.12}$$

$$s \sim (h_c - h_{av})^{-\delta} \tag{5.13}$$

$$\xi \sim (h_c - h_{av})^{-\nu}. \tag{5.14}$$

This analysis also shows that some form of critical behaviour is indeed observed in the sandpile model. It would thus seem as if the concept of critical events in the sandpile model is well justified.

In this section we have presented arguments that support the critical event concept in both earthquake physics as well as the sandpile model. As shown in the preceding sections on the application of the time-to-failure analysis, the identification of such critical events makes short time prediction of large events possible. This is encouraging since it was initially believed that systems that have SOC characteristics preclude any form of prediction.

CHAPTER 6
Conclusions

We have been concerned with two questions in this thesis. Firstly whether seismicity induced by human activity can be explained within the context of self-organised criticality. This is motivated by the success of SOC to explain certain qualitative aspects of natural tectonic earthquakes. The second question is whether there is any possibility of temporal prediction is SOC systems. At first, it would seem as if self-organised critical systems allow no such predictability due to the power-law event size distributions.

In answering these questions we followed the following route. Chapter 1 briefly discussed self-organised criticality in analogy with ordinary critical phenomena in equilibrium statistical mechanics. Several examples of systems believed to exhibit self-organised critical behaviour were mentioned and we discussed the conditions under which SOC occur.

In Chapter 2 we discussed the BTW sandpile model and its statistical properties and briefly highlighted certain known facts about the model. These include the observation that numerical simulations produce power-law event size probability distributions in the limit of slow driving. A scaling hypothesis was presented and we recalled how certain scaling relations can be derived.

In Chapter 3 we considered the critical state of the sandpile model in more detail. Firstly a more general description of the sandpile model in terms of an operator algebra due to Dhar [20] was discussed. This elegant formalism allows the calculation of certain correlation functions, notably the two-point correlation function and the correlation of heights. Still using this formalism one is also able to calculate the relative occupation of sites in the critical state. We also considered the connection between graph-theoretical concepts and the configurations of the Abelian Sandpile model. It follows that there is a one-to-one correspondence between recurrent configurations of the sandpile model and spanning trees on the lattice.

The second half of the disseration was devoted to answering the questions posed above. Chapter 4 discussed induced seismicity in general and highlighted the several correspondences that exist between seismicity and self-organised criticality. In that chapter we also provided a motivation for studying induced seismicity using the self-organised criticality framework. Two qualitative features of induced seismicity can be motivated by using the results of the analysis of the properties of the critical state of the sandpile model as done by Dhar and co-workers for the Abelian Sandpile model [20, 25]. Firstly, the possibility of small perturbations inducing large responses is justified by showing that a considerable portion of the system is close to its failure threshold. Together with this is the observation that not all perturbations induce seismic

activity. This follows from the fact that the rest of the lattice, that is not close to failure, is fairly stable against external perturbations. Secondly, results of traditional modelling approaches of the earth's crust as well as observations indicate that the stress field is correlated over long distances. Analysis of the sandpile model indicate that the sandpile heights are also long-range correlated. An important point to consider is that neither of these properties are required in the definition of self-organised criticality. They emerge from an analysis of the sandpile model and correspond to real observed features of induced seismicity. It would thus seem as if our first question can be answered in the affirmative.

We also discussed the question of bi-modal distributions in mining-induced seismic data in Chapter 4 and its possible realisation in terms of sandpile models. To this end we introduced a model that has two sets of toppling rules (directed and non-directed) that are selected randomly at each time step. This model, however, only gives slight indications of having bi-modal behaviour.

In Chapter 5 we analysed the short term temporal patterns of the sandpile model in more detail. The primary question considered is whether there is any predictive information that can be extracted from the sandpile model data. This was done in analogy with similar studies of the temporal evolution of seismicity on fault systems and mining-induced seismicity. Although one cannot account for the exact time evolution at each time step, one is able to extract enough information from the behaviour of the cumulative activity in order to make qualitative statements concerning the prediction of large events in the system. Central to the analysis of the temporal patterns is the concept of a critical event which allows the use of tools familiar from the study of continuous phase transitions. This is approach is known as a time-to-failure analysis. We gave an overview of the same analysis in tectonic [44] and mining-induced seismicity [46]. We then defined the critical event size for the sandpile model and gave a motivation for this particular choice that relies on aspects of percolation theory. The results of the analysis for the sandpile model indicate that large events are indeed preceded by a power-law increase in activity in the slow driving limit and thus the critical event hypothesis seems to apply to the model. Given the fact that the critical event hypothesis also gives one a framework within which to predict large events, it would seem as if power-law event size distributions and correlation functions in the sandpile model do not necessarily preclude the possibility of predicition of large responses to external perturbations.

Finally we consider what the open questions are related to this work. Firstly, as mentioned in Chapter 5, the exact choice for the critical event size in the sandpile model has to be determined more rigorously than we did in this work. The relation with percolation suggested here seems to

be a good starting point. Secondly, the time-to-failure analysis for the sandpile model should be extended to perform forward predictions of large events.

Thirdly, the question of modelling bi-modal behaviour in seismicity using sandpile models can be further investigated. It is not clear how to realise such bi-modal behaviour in terms of sandpile models but we suspect that it will invlove two distinct types of toppling rules. The details, however, are not yet clear.

Finally, in terms of the bigger SOC picture, there are still many open questions. As already mentioned in the Introduction to this thesis, there is as yet no single unified mathematical framework for studying SOC systems. Also, except for a few very specific models [21], the avalanche distribution exponents have not been determined analytically and questions of whether the sandpile model obeys multifractal or ordinary scaling remain unanswered.

APPENDIX A
Burning algorithm on auxiliary lattice

In this appendix we give an explicit example of constructing a new configuration on an auxiliary lattice for calculating the height correlations in the critical state of the sandpile model. We also show explicitly that the new configuration burns in exactly the same order as the configuration, on the original lattice, from which it was constructed.

4	3	2	4
3	4	3	2
1	4	2	3
3	2	3	4

Figure A.1: A recurrent configuration of the Abelian Sandpile Model

Consider the configuration in Figure A.1. Focus on the site with height $z = 1$. The auxiliary lattice is constructed by deleting the bonds of the sites above and below it. (Here we are following the prescription of Majumdar and Dhar as explained in [25] and in Chapter 3). This means that when those sites or the site with height $z = 1$ topple, no particles are exchanged between them. Effectively, they are no longer considered to be neighbouring sites. The configuration is obtained by deleting height of each of the adjacent sites (including those which bonds have been cut) so the following configuration is obtained

4	3	2	4
2	4	3	2
1	3	2	3
2	2	3	4

Figure A.2: The configuration equivalent to that in Figure A.1 on the auiliary lattice

We now apply the burning algorithm to this new configuration to determine whether it is a recurrent configuration on the auxiliary lattice.

We see that the lattice burned completely, therefore the configuration is recurrent. If we compare the burning order to that of the original configuration in Figure 3.1, we see it is exactly the same. This illustrates the assertion in the text that the burning order remains the same on the auxiliary lattice.

We should clarify one technical detail. Consider the second lattice in Figure A.3, i.e. after step 1 of burning. In the original lattice these two highlighted sites would not be able to burn

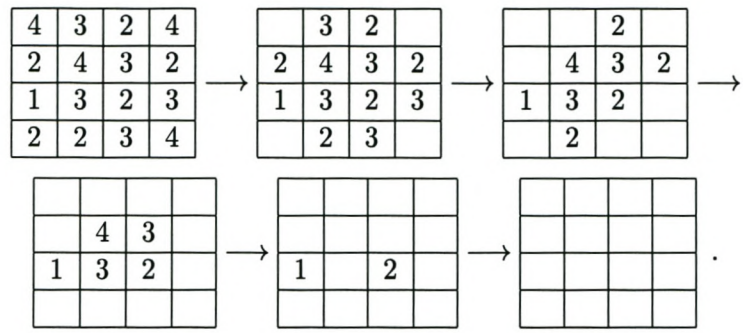

Figure A.3: An example of using the burning algorithm on the auxiliary lattice

since their heights are not strictly greater than their number of unburnt neighbours. However, on the auxiliary lattice each of these sites effectively have one unburnt neighbour, and not two, because one of the bonds was deleted and hence it is no longer considered a neighbouring site.

References

[1] P. Bak, *How Nature Works*
(Springer-Verlag, New York, 1996)

[2] H. J. Jensen, *Self-Organized Criticality*
(Cambridge University Press, Cambridge, 1998)

[3] J. M. Yeomans, *Statistical Mechanics of Phase Transitions*
(Oxford University Press, Oxford, 1992)

[4] N. Goldenfeld, *Lectures on Phase Transitions and the Renormalization Group*,
(Addison-Wesley Publishing Company , Reading, 1992)

[5] P. Bak, C. Tang and K. Wiesenfeld, Phys. Rev. A **38**, 364 (1988)

[6] Z. Olami, H. J. S. Feder and K. Christensen, Phys. Rev. Lett **68**, 1244 (1992)

[7] A. Díaz-Guilera, Phys. Rev. A **45**, 8551 (1992)

[8] L. Pietronero, A. Vespignani and S. Zapperi, Phys. Rev. Lett. **72**, 1690 (1994)

[9] H.M. Jaeger, C.-H. Liu and S.R. Nagel, Phys. Rev. Lett. **62**, 40 (1989)

[10] J. Rosendahl, M. Vekić and J. Kelly, Phys. Rev. E **47**, 1401 (1993)

[11] G. A. Held, D. H. Solina II, D. T. Keane, W. J. Haag, P. M. Horn and G. Grinstein, Phys. Rev. Lett. **65**, 1120 (1990)

[12] V. Frette, K. Christensen, A. Malthe-Sørensen, J. Feder, T. Jøssang and P. Meakin, Nature **379**, 49 (1996)

[13] D.A. Noever, Phys. Rev. E **47**, 724 (1993)

[14] E. Somfai, A. Czirok and T. Vicsek, J. Phys. A **205**, 355 (1994)

[15] B. B. Mandelbrot *Fractals and Scaling in Finance: Discontinuity, Concentration, Risk.*
(Springer, New York, 1997)

[16] S. S. Manna, J. Stat. Phys. **59**, 509 (1990)

[17] K. Christensen, H. C. Fogedby and H. J. Jensen, J. Stat. Phys. **63**, 653 (1991)

[18] L. P. Kadanoff, S. R. Nagel, L. Wu and S. Zhou, Phys. Rev. A **39**, 6524 (1989)

[19] K. Christensen and Z. Olami, Phys. Rev. E **48**, 3361 (1993)

[20] D. Dhar, Phys. Rev. Lett. **64**, 1613 (1990)

[21] D. Dhar and R. Ramaswamy, Phys. Rev. Lett. **63**, 1659 (1989)

[22] Y. -C. Zhang, Phys. Rev. Lett. **63**, 470 (1989)

[23] S. S. Manna, J. Phys. A: Math. Gen. **24**, L363 (1991)

[24] D. Dhar, Physica A **263**, 4 (1999)

[25] S. N. Majumdar and D. Dhar, J. Phys. A: Math. Gen. **24**, L357 (1991)

[26] S. N. Majumdar and D. Dhar, Physica A **185**, 129 (1992)

[27] D. V. Ktitarev, S. Lübeck, P. Grassberger, and V. B. Priezzhev, Phys. Rev. E **61**, 81 (2000)

[28] M. De Menech, A. L. Stella and C. Tebaldi, Prhys. Rev. E **58**, R2677 (1998)

[29] E. V. Ivashkevich, D. V. Ktitarev and V. B. Priezzhev, Physica A **209**, 347 (1994)

[30] S. S. Manna, D. Dhar and S. N. Majumdar, Phys. Rev. A **46**, R4471 (1992)

[31] R. Kirsten in *The South African Institute of Mining and Metallurgy Monograph Series: Increased Underground Extraction of Coal*,
S. Budavari (*ed.*) (The South African Institute of Mining and Metallurgy, 1986)

[32] B. H. G. Brady and E. T. Brown *Rock Mechanics for Underground Mining*
(Allen and Unwin Publishers, 1985)

[33] C. H. Scholz, *The Mechanics of Earthquakes and Faulting*
(Cambridge University Press, New York, 1990)

[34] J-R Grasso and D. Sornette, J. Geophys. Res. **103**, 29965 (1998)

[35] H. Kanamori and E. E. Brodsky, Physics Today **54**, 34 (June 2001)

[36] A. J. Mendecki in *Seismic Monitoring in Mines*, A. J. Mendecki (*ed.*), pp 178 - 213
(Chapman and Hall, London, 1997)

[37] D. Sornette, *Critical Phenomena in Natural Sciences*
(Springer-Verlag, Berlin, 2000)

[38] A. J. Mendecki, G. van Aswegen and P. Mountfort in *A Handbook on Rock Engineering Practice for Tabular Hard Rock Mines*, A. J. Jager and J. A. Ryder (*eds.*)
(Creda Press, Cape Town, 1999)

[39] E. Richardson and T. Jordan Bull. Seism. Soc. Am. **92(5)**, 1766 (2002)

[40] D. Sornette and J. Virieux, Nature **357**, 401 (1992)

[41] T. Hwa and M. Kardar, Phys. Rev. Lett. **62**, 1813 (1989)

[42] T. Hwa and M. Kardar, Physica D **38**, 198 (1989)

[43] Y. Ben-Zion, K. Dahmen, V. Lyakhovsky, D. Ertas and A. Agnon, Earth Planet. Sci. Lett. **172**, 11 (1999)

[44] Y. Ben-Zion and V. Lyakhovsky, Pure Appl. Geophys. **159**, 2385 (2002)

[45] D. Sornette and C. G. Sammis, J. Phys. I France **5**, 607 (1995)

[46] W. de Beer, SIMRAC Report GAP409
Department of Minerals and Energy (2000)

[47] G. Ouillon and D. Sornette, Geophys. J. Int. **143**, 454 (2000)

[48] A. Johansen and D. Sorentte, http://lanl.arxiv.org/abs/cond-mat/0003478

[49] C. J. Allègre, J. L. Mouel and A. Provost, Nature **267**, 47 (1982)

[50] D. L. Turcotte, Rep. Prog. Phys. **62**, 1377 (1999)

[51] B. K. Chakrabarti and L. G. Benguigui, *Statistical Physics of Fracture and Breakdown in Disordered Systems*
(Oxford University Press, Oxford, 1997)

[52] S. Pradhan and B. K. Chakrabarti, Phys. Rev. E **65**, 016113-1 (2001)